.

SCUOLA INTERNAZIONALE SUPERIORE DI STUDI AVANZATI

SISSA Digital Library

Hyperpolarization-activated current Ih in mouse trigeminal sensory neurons in a transgenic mouse model of familial hemiplegic migraine type-1

Original
Hyperpolarization-activated current Ih in mouse trigeminal sensory neurons in a transgenic mouse model of familial hemiplegic migraine type-1 / Eroli, F., Vilotti, S., van den Maagdenberg, A.M.J.M., Nistri, A.. - In: NEUROSCIENCE. - ISSN 0306-4522. - 351:May(2017), pp. 47-64. [10.1016/j.neuroscience.2017.03.033]

Availability:
This version is available at: 20.500.11767/56283 since: 2017-08-22T09:55:04Z

Publisher:

Published
DOI:10.1016/j.neuroscience.2017.03.033

Terms of use:

Testo definito dall’ateneo relativo alle clausole di concessione d’uso

Publisher copyright

note finali coverpage

(Article begins on next page)

16 October 2026

SCUOLA INTERNAZIONALE SUPERIORE DI STUDI AVANZATI

SISSA Digital Library

Publication title: Current Pharmaceutical Design

Citation	*Eroli, F., Vilotti, S., van den Maagdenberg, A.M.J.M., Nistri, A. Hyperpolarization-activated current /(h) in mouse trigeminal sensory neurons in a transgenic mouse model of familial hemiplegic migraine type-1 (2017) Neuroscience, 351, pp. 47-64.*
Link to the Publisher *(es. DOI)*	DOI: 10.2174/1381612822666161214151051
Publisher	Elsevier
Version ***(Postprint, Preprint)***	Postprint
Terms of Use *(Licence)*	Embargo 12 mesi CC BY NC ND

HYPERPOLARIZATION-ACTIVATED CURRENT I_H IN MOUSE TRIGEMINAL SENSORY NEURONS IN A TRANSGENIC MOUSE MODEL OF FAMILIAL HEMIPLEGIC MIGRAINE TYPE-1

FRANCESCA EROLI [a] , SANDRA VILOTTI [a], ARN M. J. M. VAN DEN MAAGDENBERG [b,c] , ANDREA NISTRI [a*]

[a]Neuroscience Department, International School for Advanced Studies (SISSA), Trieste, Italy

[b]Department of Neurology, Leiden University Medical Centre, Leiden, Netherlands

[c] Department of Human Genetics, University Medical Centre, Leiden, Netherlands

* Corresponding author. Address: SISSA, Via Bonomea 265, 34136, Trieste, Italy. Fax: +39-040-3787702.

E-mail addresses: feroli@sissa.it (F. Eroli), vilotti@sissa.it (S. Vilotti), A.M.J.M.van_den_Maagdenberg@lumc.nl (A. M. J. M. van den Maagdenberg), nistri@sissa.it (A. Nistri).

Abbreviations: α,β-meATP, α,β -methylene-ATP; AP, action potential; DRG, dorsal root ganglia; CGRP, calcitonin gene-related peptide; FHM1, familial hemiplegic migraine type-1; HCN, hyperpolarization-activated cyclic nucleotide-gated channel; I_h, hyperpolarization-activated current; KI, knock-in; MF, multiple-firing; NS, non-spiking; P2X3, purinergic P2X3 receptor; SS, single-spike; TEA, tetraethylammonium chloride; TG, trigeminal ganglion; TRPV1, transient receptor potential vanilloid-1; V_{rev}, reversal potential; WT, wildtype.

http://dx.doi.org/10.1016/j.neuroscience.2017.03.033 (Available online 29 March 2017)

Abstract

Transgenic knock-in (KI) mice that express $Ca_V2.1$ channels containing an R192Q gain-of-function mutation in the α_{1A} subunit known to cause familial hemiplegic migraine type-1 in patients, exhibit key disease characteristics and provide a useful tool to investigate pathophysiological mechanisms of pain transduction. Previously, KI trigeminal sensory neurons were shown to exhibit constitutive hyper-excitability due to up-regulation of ATP-gated P2X3 receptors that trigger spike activity at a more negative threshold. This implies that intrinsic neuronal conductances may shape action potential generation in response to ATP, which could act as a mediator of migraine headache. Here we investigated whether the hyperpolarization-activated conductance I_h, mediated by hyperpolarization activated cyclic nucleotide-gated channels (HCN), contributes to sub-threshold behavior and firing in wild-type (WT) and KI trigeminal ganglia (TG) neurons. Whereas most WT and KI trigeminal neurons expressed I_h current, blocked by the specific inhibitor ZD7288, it was smaller in KI neurons despite similar activation and deactivation kinetics. HCN1 and HCN2 were the most abundantly expressed subunits in TG, both *in situ* and in culture. In KI TG neurons, HCN2 subunits were pre-dominantly present in the cytoplasm, not at the plasma membrane, likely accounting for the smaller I_h of such cells. ZD7288 hyperpolarized the membrane potential, thereby raising the firing threshold, and prolonging the spike trajectory to generate fewer spikes due to P2X3 receptor activation. The low amplitude of I_h in KI TG neurons suggests that down-regulation of I_h current in sub-threshold behavior acts as a compensatory mechanism to limit sensory hyper-excitability, manifested under certain stressful stimuli.

Key words: trigeminal ganglion, excitability, P2X3, ZD7288, CGRP, HCN.

INTRODUCTION

Familial hemiplegic migraine type-1 (FHM1) is a rare monogenic subtype of migraine with aura (Headache Classification Committee of the International Headache Society (IHS), 2013) that is caused by specific missense mutations in the CACNA1A gene, which encodes the pore-forming α_{1A} subunit of neuronal voltage-gated $Ca_V2.1$ (P/Q-type) calcium channels (Ophoff et al., 1996; Ferrari et al., 2015; Tolner et al., 2015). A transgenic knock-in (KI) mouse model of FHM1 expressing the R192Q missense mutation shows a gain-of-function phenotype of mutated $Ca_V2.1$ channels with increased neurotransmission and susceptibility to cortical spreading depression (van den Maagdenberg et al., 2004; Eikermann-Haerter et al., 2009; Tottene et al., 2009), heightened trigeminal sensory neuron firing (Hullugundi et al., 2014; Marchenkova et al., 2016a), and head pain (Chanda et al., 2013). In particular, these KI mice exhibit intense photophobia and unilateral head pain only under stressful conditions in analogy to human attacks of migraine (Chanda et al., 2013). The issue of what controls trigeminal sensory excitability in between migraine attacks remains unclear.

Trigeminal ganglia (TG) of R192Q KI mice show a selective potentiation of neuronal P2X3 receptor-mediated currents (Nair et al., 2010), which results in a lower firing threshold and a larger number of spikes in response to P2X3 activation by ATP agonists, whereas capsaicin-sensitive transient receptor potential vanilloid-1 (TRPV1) receptors (Julius and Basbaum, 2001; North, 2003) are not facilitated (Nair et al., 2010). Furthermore, an enhanced release of the neuropeptide calcitonin gene-related peptide (CGRP; (Ceruti et al., 2011), which is believed to be a mediator that triggers headache attacks (Olesen et al., 2004; Messlinger et al., 2011), was observed in R192Q KI TG, thus contributing to the observed up-regulation of P2X3 receptors (Fabbretti et al., 2006; Hullugundi et al., 2013).

The KI phenotype, therefore, recapitulates two functional changes in TG activity: up-regulation of $Ca_V2.1$ channels and P2X3 receptors. Both targets are expected to operate in a range of membrane potentials below the threshold for neuronal firing. Below threshold excitability is regulated by a combination of (de) activation of certain neuronal conductances (Bean, 2007) ultimately responsible for the speed and extent of depolarization that a chemical signal like ATP (which acts on P2X3 receptors) might produce. Within this framework, the hyperpolarization-activated current (I_h), a mixed cationic conductance that is activated by membrane hyperpolarization, may be viewed as a key regulator of cellular excitability and electrical responsiveness of cells (reviewed in Biel et al., 2009). I_h channels belong to the hyperpolarization-activated cyclic nucleotide-gated (HCN) channel superfamily (Robinson and Siegelbaum, 2003; Hofmann et al., 2005). Four subunits of mammalian HCN channels (HCN1–4) have been identified (Ludwig et al., 1998; Santoro et al., 1998) that have distinct properties (Moosmang et al., 2001; Stieber et al., 2003). Functional HCN channels can be assembled as homomeric or heteromeric tetramers, the latter being HCN1 and HCN2 as observed in vivo (Much et al., 2003). In the peripheral nervous system, all four HCN subtypes are expressed, HCN1 and HCN2 being most abundantly expressed (Chaplan et al., 2003; Kouranova et al., 2008; Hatch et al., 2013). In dorsal root ganglia (DRG) and TG, HCN1 is found mainly in medium- to large-size non-nociceptive neurons (Tu et al., 2004; Kouranova et al., 2008; Hatch et al., 2013), apart from a small subpopulation of cold-sensitive neurons (Momin et al., 2008; Orio et al., 2009). HCN2 subunits are expressed in DRG and TG neurons of all sizes (Tu et al., 2004; Matsuyoshi et al., 2006; Kouranova et al., 2008; Hatch et al., 2013), especially in small nociceptive neurons, and play a critical role in inflammatory and neuropathic pain (Emery et al., 2011, 2012). The distribution of HCN3 and HCN4 sub-units in sensory neurons is less clear and only a relatively small proportion of TG sensory neurons express these proteins. Consistent with this, I_h is differentially expressed in a subpopulation of primary sensory neurons (Scroggs et al., 1994) in which it exerts a prominent role in shaping the electrical behavior (Momin et al., 2008; Orio et al., 2009; Cho et al., 2011). HCN channels play a role in generating hyperexcitability of peripheral nerve fibers and DRG neurons in various pain models (Chaplan et al., 2003; Tu et al., 2004; Emery et al., 2011; Weng et al., 2012). In particular, in chronic and inflammatory pain, I_h current density and the rate of activation are increased in TG and DRG cells (Chaplan et al., 2003; Yao et al., 2003; Tsuboi et al., 2004; Kitagawa et al., 2006). The selective HCN blocker ZD7288 is known to depress pain behavior and ectopic neuronal firing both *in vivo* and *in vitro* (Chaplan et al., 2003; Lee et al., 2005; Emery et al., 2011).

The aim of the present study was to compare the expression of I_h in wild-type (WT) and R192Q KI mice TG neurons and assess its impact on neuronal excitability elicited by either activation of P2X3 receptors with the selective agonist α,β-methylene-ATP (α,β -meATP), or TRPV1 receptors by capsaicin.

EXPERIMENTAL PROCEDURES

Animals and primary TG cultures

All experimental procedures were carried out in accordance with the guidelines of the Italian Animal Welfare Act and approved by the Scuola Internazionale Superiore di Studi Avanzati (SISSA) ethics committee (prot. 3599, 28 May 2012). All efforts were made to minimize the number of animals used for the experiments and their suffering. Homozygous $Ca_V2.1$ R192Q KI and WT mouse littermates (van den Maagdenberg et al., 2004) of either sex were used for the study. Genotyping was performed by PCR as previously reported (van den Maagdenberg et al., 2004). Trigeminal ganglia (TG) primary cultures were obtained from mice at postnatal day 14 (P14) rapidly decapitated under i.p. urethane-anesthesia (10% solution, 0.1 mL injection) as previously described (Simonetti et al., 2006), and incubated (37 LC, 5% CO_2) for 24 h before use. Ganglion tissue samples and cultures were collected and processed in parallel for R192Q KI and WT mice.

Western blot

Mouse TG ganglia or cultures were homogenized in ice-cold lysis buffer containing 50 mM Tris–HCl pH 7.5, 150 mM NaCl, 0.1% Nonidet P (NP)-40, 0.1% sodium deoxycholate, 0.1% SDS, 2 mM EDTA plus protease inhibitors mixture (Complete, Roche Applied Science, Basel, Switzerland). The procedure was essentially the same as described earlier (Fabbretti et al., 2004). The following polyclonal antibodies were used: anti-HCN1 (1:1000, rabbit #APC-056), anti-HCN2 (1:1000, rabbit #APC-030), anti-HCN3 (1:500, rabbit #APC-057), anti-HCN4 (1:1000, rabbit #APC-052), all purchased from Alomone Laboratory (Jerusalem, Israel) and isoform-specific anti- β -actin (1:5000; A5441, Sigma Milan, Italy), and anti- β -tubulin III (1:3000; T5076, Sigma). Secondary antibodies were conjugated with horseradish peroxidase and their reaction was visualized with the ECL detection system (Amersham Biosciences, Piscataway, NJ, USA) and recorded with the Alliance 4.7 (UVITEC, Cambridge, UK) digital imaging. Data were normalized with respect to levels of β-tubulin III or β -actin. The amount of loaded proteins was in the 20–50 μg/mL range. The specificity of the antibodies used in this study was previously validated (Han et al., 2002; Chaplan et al., 2003; Much et al., 2003; Cho et al., 2011; Acosta et al., 2012). Specificity of the HCN antibodies was further confirmed by Western blots of mouse tissue (for details see Fig. 7). Olfactory bulb was used as a positive control tissue for HCN1-3 (Notomi and Shigemoto, 2004). Heart was used as positive control for HCN4 (Moosmang et al., 2001). Liver was used as negative control tissue, where no HCN isoforms were detected as previously reported (Arroyo et al., 2006). To remove the N-glycosylation moiety of the protein, lysates were incubated with Peptide-N- Glycosidase F (PNGase F) according to the manufacturer's instructions (1000 U/reaction; New England Bio-labs, Frankfurt, Germany).

Cell surface biotinylation assay

For biotinylation experiments, cells previously washed with cold phosphate-buffered saline (PBS) were treated with 0.5 mg/mL EZ-link^{TM} Sulfo-NHS-LC-Biotin (Thermo Scientific, Rockford, Illinois, USA) as formerly described (Fabbretti et al., 2006). Subsequently, the cells were washed twice with 200 mM glycine in cold PBS and twice with cold PBS to inactivate and remove the excess biotin, respectively. The cells were then lyzed with lysis buffer containing 50 mM Tris–HCl pH 7.5, 150 mM NaCl, 0.1% Nonidet P (NP)-40, 0.1% sodium deoxycholate, 0.1% SDS, 2 mM EDTA plus protease inhibitors (Roche) for 30 min at 4 LC. Cell lysates were centrifuged at 13,000g at 4 LC for 15 min. Two mg of the supernatant were incubated with 50 ll Streptavidin Sepharose High Performance beads (GE Healthcare, Uppsala, Sweden) for 2 h at 4 LC, and the remaining supernatant was kept as the input. The beads were subsequently washed five times with lysis buffer before elution with 50 µl of 2 sample buffer plus 100 mM dithiothreitol. Biotinylated and input samples were processed for Western blotting using antibodies against HCN1-4 (1:1000). Positive control for biotinylation assay of membrane expression was obtained by checking the surface expression of the transferrin receptor (Vilotti et al., 2013) detected with an antibody purchased from Santa Cruz Biotechnology (1:1000, Heidelberg, Germany).

Immunohistochemistry

For immunohistochemistry, adult (P30) mice were deeply anesthetized with an intraperitoneal injection of urethane (0.3 mL of 1 g/mL; Sigma) and transcardially perfused with PBS followed by 4% paraformaldehyde. Tissues were isolated and post-fixed for 1 h, then cryo-protected for 24 h before being embedded in 100% Neg-50 frozen section medium (Thermo Fisher Scientific, Waltham, MA, USA). Each experiment was performed on, on average, 5 cryostat-cut serial longitudinal slices (12 µm-thick) sampled every 70 µm, thus covering the entire ganglion. After cutting, sections were air-dried for 1 h and washed three times for 5 min with PBS. Ganglion sections or TG culture samples were pre-incubated for 1 h in blocking solution (5% normal goat serum +5% BSA + 0.1% Triton X-100 in PBS). TG sections and primary cultures were incubated overnight at 4 LC or 90 min at room temperature, respectively, with primary antibodies against HCN1, HCN2, HCN3 or HCN4 (all 1:500; Alomone Laboratory), and β-tubulin III (1:1000; Sigma), diluted in blocking buffer. Secondary antibodies conjugated with Alexa Fluor-488 or Alexa Fluor-594 (1:500; goat anti-mouse and anti-rabbit; Invitrogen, Milan, Italy) were used. Nuclei were counterstained with DAPI (Sigma). Images from whole-ganglion sections and cell cultures were visualized with a Leica TCS SP2 confocal microscope (Wetzlar, Germany) or a Zeiss Axioskop fluorescence microscope (Zurich, Switzerland).

The peri-membrane region was defined as the one within 5 µm from the cell surface. Unless otherwise stated, an average of 500 cells was analyzed in each test, and data are the mean of three independent experiments. To verify the specificity of the immunohistochemical reaction, every staining was controlled by omitting the primary antibody in the incubation fluid. Pre-absorption controls were performed for all HCN primary antibodies using their specific blocking peptides (ratio 100:1 peptide/antibody concentration), supplied by the antibody manufacturers. Blocking peptides were re-suspended in sterile water and then incubated in PBS containing 1% BSA and 3% normal goat serum, with primary antibodies, at 4 LC. Sections incubated with antibodies alone versus blocked antibodies were compared.

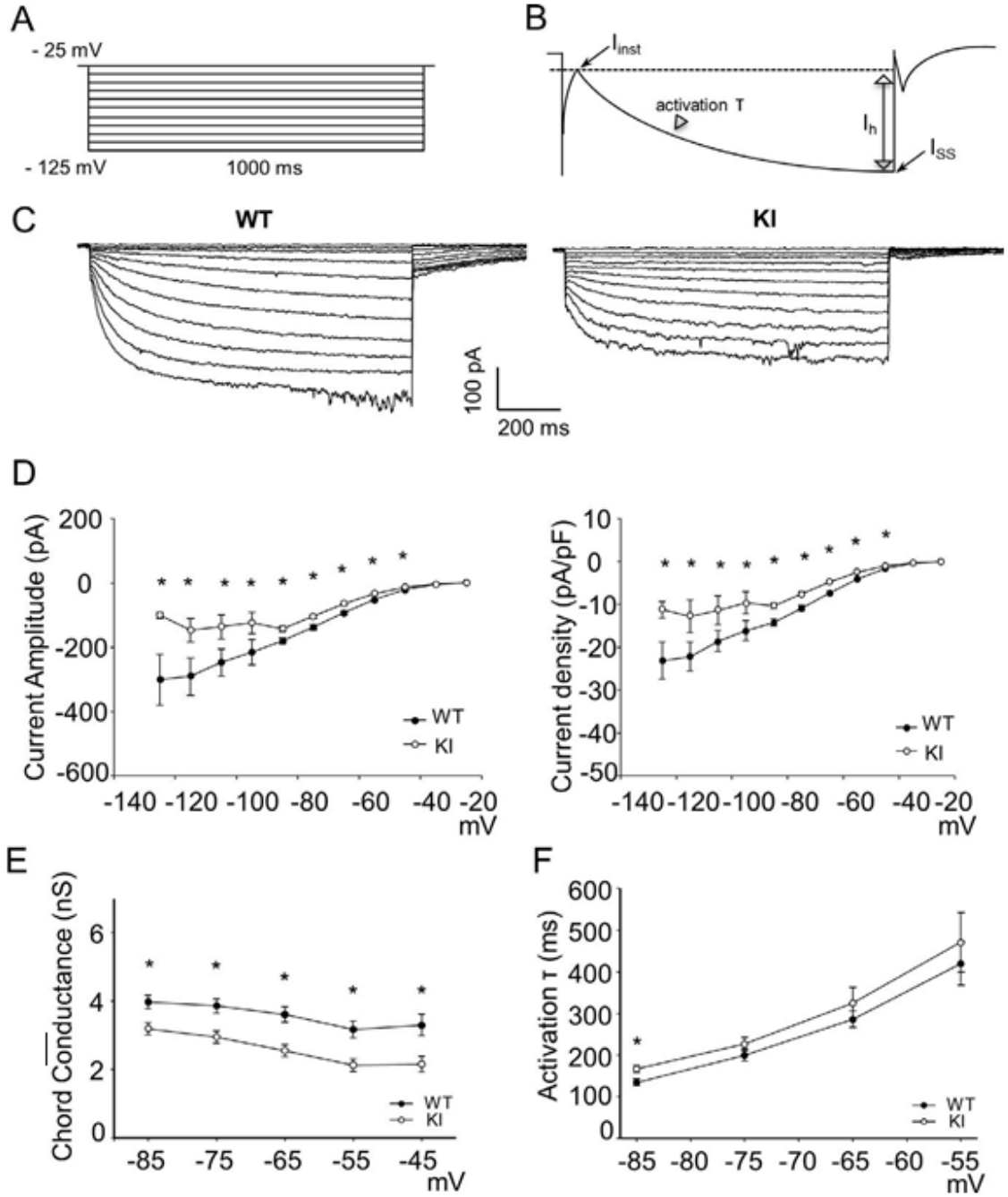

Fig. 1. Inward current relaxations of R192Q KI and WT TG neurons. (A) Schematic protocol of current activation. Recorded inward relaxations were activated by hyperpolarization from –25 mV holding potential to –125 mV final voltage level in –10 mV steps. (B) Schematic illustration of parameters for current relaxation measurements in trigeminal ganglia (TG) neurons. Current amplitude was calculated as the difference between I_{ss} and I_{inst} for each voltage step. (C) Representative traces of recorded inward currents from KI and WT TG neurons. (D) Left panel, I-V curves of average amplitude values of inward currents plotted against the membrane potential in KI (open circles, *n* = 112 up to -85 mV, and *n* = 8 up to -125 mV) and WT (filled circles, *n* = 122 up to -85 mV, and *n* = 10 up to -125 mV) neurons; at -45 mV *p = 0.007, at -55 mV *p = 0.0006, at -65 mV *p = 0.0004, at -75 mV *p = 0.0004, at

–85 mV *p = 0.001, at -95 mV *p = 0.03, at -105 mV *p = 0.05, at -115 mV *p = 0.05, at -125 mV *p = 0.05, Mann–Whitney rank sum test. Right panel, I-V curves of average current amplitude values normalized to cell capacitance in KI (open circles, *n* = 112 up to -85 mV, and *n* = 8 up to -125 mV) and WT (filled circles, *n* = 122 up to -85 mV, *n* = 10 up to -125 mV) neurons; at -45 mV *p = 0.001, at -55 mV *p = 0.00005, at -65 mV *p = 0.00003, at -75 mV *p = 0.00004, at –85 mV *p = 0.0002, at –95 mV *p = 0.02, at –105 mV *p = 0.03, at –115 mV *p = 0.01, at –125 mV *p = 0.04, Mann–Whitney rank sum test. (E) Average chord conductance values plotted against the membrane potential in KI and WT neurons (*n* = 104, 107, respectively); at –45 mV *p = 0.02, at –55 mV *p = 0.004, at –65 mV *p = 0.001, at –75 mV *p = 0.003, at –85 mV *p = 0.006, Mann–Whitney rank sum test. (F) Average time constant (s) values of current activation as a function of membrane voltage. The values of s were obtained by fitting the inward currents with a single exponential equation as described in Methods. KI, *n* = 37; WT, *n* = 22; *p = 0.03, Mann–Whitney rank sum test.

Electrophysiology and data analysis

Patch-clamp experiments were performed as previously reported (Nair et al., 2010; Hullugundi et al., 2013). After 24 h in culture, trigeminal neurons were superfused continuously (2 mL/min) with physiological solution containing (in mM): 152 NaCl, 5 KCl, 1 $MgCl_2$, 2 $CaCl_2$, 10 glucose, and 10 HEPES (pH adjusted to 7.4 with NaOH). Cells were patch-clamped in the whole-cell configuration using an Axopatch 200B amplifier (Molecular Devices, Sunny-vale, CA, USA) and acquired by means of a DigiData 1200 Interface and pClamp 8.2 software (Molecular Devices, Sunnyvale, CA, USA). Cellular responses were filtered at 1 or 10 kHz under voltage- or current-clamp conditions, respectively (Hullugundi et al., 2013, 2014). Recordings were performed on small- and medium-size neurons (15–25 mm) with a capacitance less than 22 pF, both in KI and WT cultures. In voltage-clamp experiments, the pipette resistance was 3–4 MΩ when filled with the following solution (in mM): 140 KCl, 0.5 $CaCl_2$, 2 $MgCl_2$, 2 Mg_2ATP_3, 2 GTP, 10 HEPES, and 10 EGTA (pH adjusted to 7.2 with KOH). The liquid junction potential calculated with JP calculator of pClamp software was 3.5 mV and all data were corrected accordingly. In accordance with standard protocols (Maccaferri et al., 1993; Momin et al., 2008), I_h was activated by applying a series of hyperpolarizing voltage steps, starting from a holding potential of –25 mV to a final voltage of –125 mV in –10 mV increments (duration 1000 ms). I_h amplitude was calculated as the difference in current between instantaneous current (I_{inst}) at the beginning and steady state current (I_{ss}) at the end of each 1-s voltage step, respectively (see Fig. 1 B). These data were not obtained in the presence of pharmacological blockers to suppress multiple voltage-activated conductances because the goal was to compare WT and KI responses under control conditions and the use of pharmacological inhibitors might have differential impact on the two phenotypes. While the use of standard physiological solution did not preclude the occasional emergence of unclamped components upon return to a depolarized holding potential (see for instance Halliwell and Adams, 1982), this phenomenon was, however, uncommon (4% of the present recordings) presumably because of the heterogeneity of Na^+ and Ca^{2+} conductances expressed by TG neurons (Spigelman and Puil, 1989; Kim and Chung, 1999; Fioretti et al., 2011) with consequential differences in firing patterns and spike latency (Hullugundi et al., 2014) and dishomogeneous reactivation on depolarization. This issue, that was amply investigated in earlier neurophysiological studies of trigeminal sensory neurons *in vivo* (Puil et al., 1987) and *in vitro* (Puil et al., 1988; Spigelman and Puil, 1989), was not a major limitation to the use of standard voltage jump protocols for I_h. In addition, it seems likely that long-lasting holding at –25 mV level contributed to rundown of the fast inward currents. Finally, the jump protocol might have modulated voltage-sensitive potassium currents (Puil et al., 1987) that operate against the activation of inward conductances.

The time constant values for I_h activation (activation τ), calculated at each step of membrane potentials between –85 mV and –55 mV, were obtained by fitting the first 450 ms with a single exponential equation (Clampfit 10, Molecular Devices). Chord conductance (G) was calculated at each voltage step using the equation: $G = I/(V_m - V_{rev})$, where Vm is the membrane potential, I is the corresponding current amplitude and Vrev is the reversal potential (–37 mV) experimentally determined by Cho et al. (2011) for trigeminal sensory neurons.

In current-clamp experiments, the pipette resistance was 4–5 MΩ when filled with the following solution (in mM): 125 K-gluconate, 5 KCl, 2 $MgCl_2$, 2 Mg_2ATP_3, 10 HEPES, and 10 EGTA (pH adjusted to 7.2 with KOH). Cells were held at –70 mV, a value corrected for the calculated liquid junction potential of 14.6 mV. Input resistance in current-clamp experiments was measured by applying hyperpolarizing pulses of –5 pA, while the cell capacitance from the whole-cell was estimated capacitance facility. In accordance with previous studies (Nair et al., 2010; Hullugundi et al., 2014), P2X3 receptor selective agonist α,β-meATP (Sigma) was applied for 2 s at a concentration of 10 μM to produce near-maximal P2X3 receptor activation (Sokolova et al., 2006). Capsaicin (Sigma) was applied for 3 s at a concentration of 1 μM to evoke TRPV1 receptor-mediated responses (Simonetti et al.,2006; Nair et al., 2010; Hullugundi et al., 2014). The number of spikes was calculated using Clampfit, while action potential (AP) threshold was determined using the automated threshold detection algorithm of Axograph software (Axograph X, Berkeley, CA, USA), that measures the AP threshold from the first time derivative (dV/dt) of the voltage (Platkiewicz and Brette, 2010). Parameters used for detecting threshold values were then kept constant for all analyzed traces; data were consistent with the values reported in literature (Sekerli et al., 2004; Marchenkova et al., 2016a).

Drugs

Drugs were perfused using a fast superfusion system (Rapid Solution Changer RSC-200; BioLogic Science Instruments, Claix, France). The following chemicals were used: ZD7288 (50 μM as indicated by Harris and Constanti, 1995), linopirdine dihydrochloride (linopirdine, 30 μM; Aiken et al., 1995; Passmore et al., 2003), BIBN 4096 (BIBN, 50 nM; Olesen et al., 2004), AC187 (1 μM; Jhamandas et al., 2003), tetraethylammonium chloride (TEA, 10 mM; Battefeld et al., 2012), and CGRP (2 μM; Fabbretti et al., 2006; Hullugundi et al., 2013). Chemicals were dissolved in distilled water except for BIBN that was dissolved

in DMSO, as suggested by the datasheet of the manufacturer. ZD7288, linopirdine, BIBN and AC187 were purchased from Tocris Bioscience (Bristol, UK), whereas TEA and CGRP were purchased from Sigma–Aldrich (Saint Louis, MO, USA).

Statistics

Data are expressed as mean ± SE where *n* indicates the number of independent experiments or the number of investigated cells, as indicated in figure legends. The nonparametric Mann–Whitney rank sum test, or the Student's *t*-test was used for statistical analysis after establishing the data distribution with the ANOVA test (Matlab; Sigma Plot and Sigma Stat Software, Chicago, IL, USA); the chi-square test was used when analyzing percent distributions. A *p*-value of < 0.05 was accepted as indicative of a statistically significant difference.

RESULTS

Characterization of I_h current in TG neurons of R192Q KI and WT mice

Voltage-clamp experiments were performed to compare characteristics of I_h in R192Q KI and WT neurons. Using standard protocols (Momin et al., 2008), recorded inward relaxations were activated by hyperpolarization from –25 mV holding potential to –125 mV final voltage level in –10 mV incrementing steps: the current amplitude was measured as the peak current plateauing at each voltage step (schematic protocol in Fig. 1A, B). Fig. 1C shows representative traces from KI and WT neurons. The analysis of these inward currents revealed significantly smaller current amplitude in KI neurons compared to WT (Fig. 1D, left panel). Current activation was observed from values more negative than –40 mV, as shown in Fig. 1 D. In 4% of recorded cells, the off response was contaminated by unclamped inward components (including Na^+ spikes) when the test potential was –75 mV or –85 mV: this phenomenon was previously shown with hippocampal pyramidal neurons in normal physiological solution in absence of tetrodotoxin or any other Na^+ blocker (Halliwell and Adams, 1982) and represents occasional lack of isopotential conditions under large voltage shifts. Normalization of responses to cell capacitance showed similar results compared to current amplitude (Fig. 1D), consistent with the similar neuronal diameters in KI and WT ganglia (Nair et al., 2010).

On the basis of the apparent absence of slow inward relaxations at –40 mV (Fig. 1 D) and the I_h reversal value (–37 mV) determined for trigeminal sensory neurons (Cho et al., 2011), chord conductance was calculated (cf. Methods section) and plotted against the voltage step, demonstrating modest voltage-dependence with smaller chord conductance values of KI compared to WT neurons (Fig. 1 E). Time constants of current activation were measured at voltage steps from –55 mV to –85 mV with similar values for KI and WT neurons, except for τ values measured at –85 mV that was slightly slower in KI cells (Fig. 1 F). This finding suggests that the smaller inward current observed in KI TG cells may depend on a change in the HCN channel expression mediating I_h current.

We also run a series of control experiments to estimate neuronal leak conductance calculated by applying ±5 mV steps and measuring the corresponding current responses at –70 mV holding potential (Fig. 2 A). We then constructed *I/V* plots by linear extrapolation of these responses that assumed a linear (ohmic) behavior (Fig. 2 B). The estimated leak values were then subtracted from the observed amplitude of the I_h at various membrane potentials and plotted as shown in Fig. 2 C. It was apparent that there was no significant difference in the calculated values for I_h. On average, the mean input resistance (at -25 mV holding potential) was 1.2 ± 0.3 (n = 10) and 1.2 ± 0.2 (n = 8) GΩ for WT and KI neurons, respectively. These values were retained (1.3 ± 0.2 and 1.2 ± 0.3 GΩ, respectively) in the presence of ZD7288.

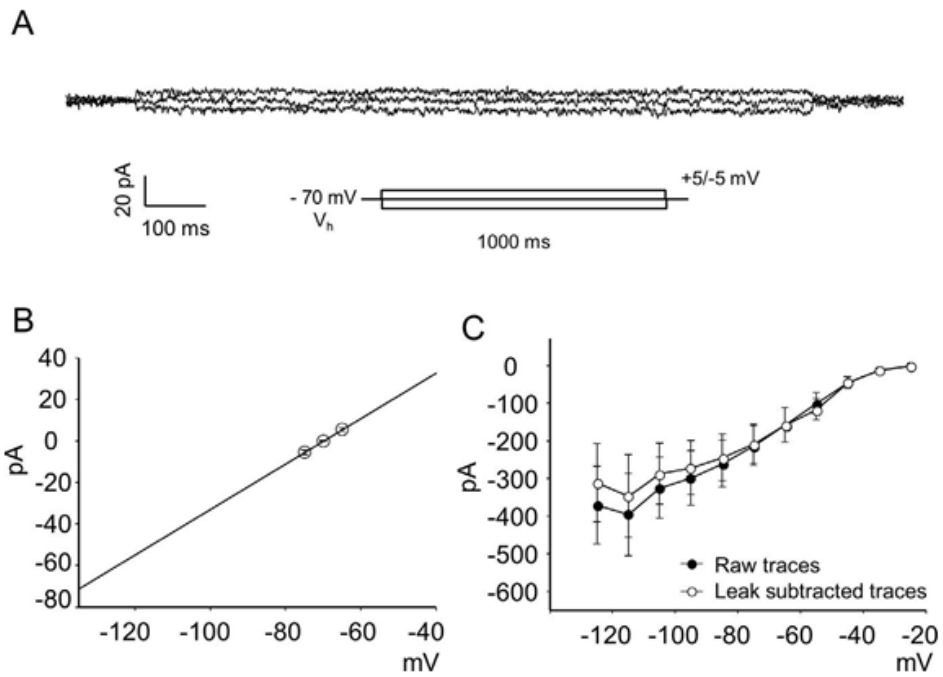

Fig. 2. Estimate of leak conductance. (A) sample traces of responses (at –70 mV holding potential) of WT trigeminal neuron tested with ±5 mV steps to assess the cell passive membrane properties. (B) *I/V* plot of measured responses (see open symbols in which the standard error is comprised within the symbol; *n* = 11 cells) used to extrapolate the linear (ohmic) behavior of these cells (see straight line). (C) *I/V* plots for I_h observed on the same cells as uncorrected slow inward rectifications (filled circles; *n* = 6) or after leak subtraction (*n* = 6).

To confirm the identity of the recorded inward relaxation as I_h, a range of blockers were applied to pharmacologically dissect I_h current from other currents. Application of selective HCN blocker ZD7288 (50 μM, 5 min; BoSmith et al., 1993; Harris and Constanti, 1995; Cho et al., 2011) almost completely abolished I_h (95% reduction) in both KI and WT neurons, as exemplified in Fig. 3 A, B, leaving a minimal, residual inward current at –85 mV (on average –11.3 ± 7.8 pA in WT, *n* = 10, and –9 ± 6.2 pA in KI, *n* = 8). Furthermore, application of non-selective K^+-channel blocker TEA (10 mM, 5 min; Battefeld et al., 2012) did not significantly reduce I_h amplitude (Fig. 3 C) as expected from HCN-mediated currents that are known to be insensitive to millimolar concentrations of this blocker (Ludwig et al., 1998; Funahashi et al., 2003; Battefeld et al., 2012). To test for the presence of M-type K^+ current (KCNQ-mediated current) that could be activated in our range of voltage steps, we applied the selective M-current blocker linopirdine (Aiken et al., 1995; Passmore et al., 2003). Recorded inward currents were not inhibited by linopirdine (30 μM, 5 min) as shown in Fig. 3 D for KI and WT neurons, thus showing no apparent involvement of the M-current.

These findings strongly suggest that the inward relaxations evoked by the present protocols were due to I_h activity, with minor contribution by other currents, including leak components. I_h could be recorded from the vast majority of recorded neurons (92% of KI neurons expressed I_h, 90.7% of WT neurons expressed I_h, *n* = 108; *n* = 113).

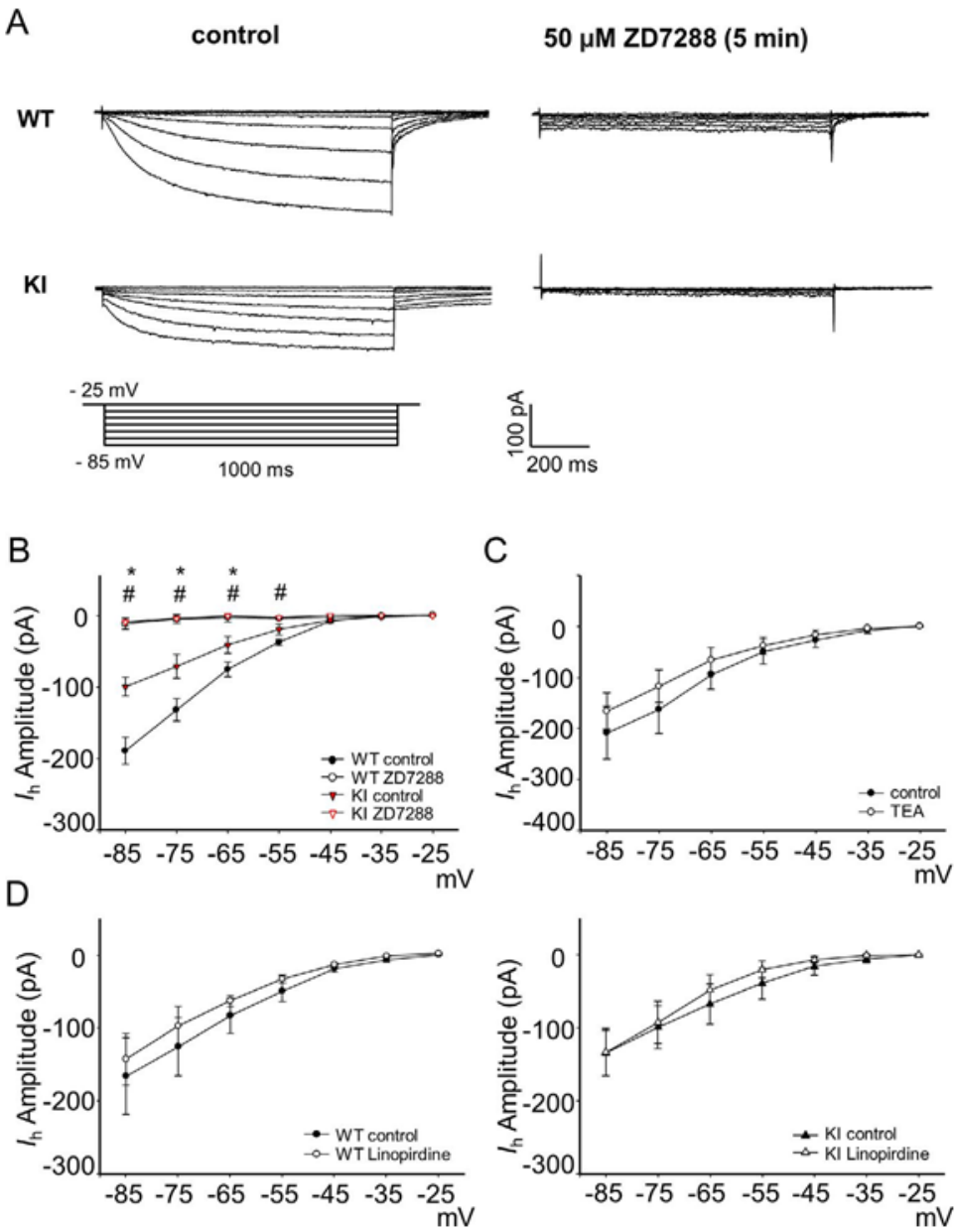

Fig. 3. Pharmacological identification of inward relaxations as I_h current manifestation. (A) representative traces of inward relaxations recorded from KI and WT trigeminal ganglion (TG) neurons in control condition (left) and after a 5-min application of ZD7288 (50 μM, right) to the same cells. The selective block by ZD7288 identified these responses as due to I_h current. (B) *I-V* curves of average I_h current amplitude measured at each voltage step from KI and WT neurons in control and after ZD7288 (KI, n = 8; WT, n = 10). # indicates significant difference between WT control and WT ZD7288; * indicates significant difference between KI control and KI ZD7288; at –55 mV #p = 0.0002, at –65 mV #p = 0.0004, at –75 mV #p = 0.000008, at –85 mV #p = 0.0002, Mann–Whitney rank sum test; at –65 mV *p = 0.03, at –75 mV *p = 0.008, at –85 mV *p = 0.001, paired t-test. (C) *I-V* curves of average *Ih* amplitude recorded from WT neurons in control and after a 5-min application of 10 mM TEA to the same cells (n = 5). (D) I–V curves of average I_h current amplitude recorded from WT (left panel) and KI neurons (right panel) in control and after a 5-min application of 30 μM linopirdine (KI, n = 6; WT, n = 4).

CGRP did not affect I_h currents of TG neurons

Enhanced CGRP levels in R192Q KI trigeminal ganglia (Ceruti et al., 2011; Fioretti et al., 2011) lead to constitutive potentiation of P2X3 receptors in KI TG neurons (Fabbretti et al., 2006; Ceruti et al., 2011; Hullugundi et al., 2013). Therefore, we investigated whether CGRP might modulate the I_h current in KI neurons. In voltage-clamp experiments, prolonged application of CGRP (2 μM, 2 or 24 h; Fabbretti et al., 2006; Hullugundi et al., 2013) did not change I_h current amplitude in KI or WT neurons (Fig. 4A, B). Subsequently, we explored the effect of constitutive release of CGRP by applying the selective CGRP receptor antagonist BIBN (50 nM, 24 h; Olesen et al., 2004). Fig. 4 C shows that no significant change was observed in I_h

current amplitude after BIBN application. CGRP belongs to the calcitonin gene peptide superfamily comprising other peptides, such as calcitonin and amylin (Wimalawansa, 1997). CGRP presents a large affinity for the amylin receptors as well, with potentially overlapping biological effects (Wimalawansa, 1997; Walker and Hay, 2013) so to verify any involvement of amylin receptors in I_h modulation, we studied the action of selective amylin receptor antagonist AC187 (1 μM; Jhamandas et al., 2003). As a 24-h pretreatment of KI and WT TG cultures with AC187 failed to modify I_h amplitude (Fig. 4D), this suggests that the observed I_h depression in KI neurons was not directly related to the CGRP pathway.

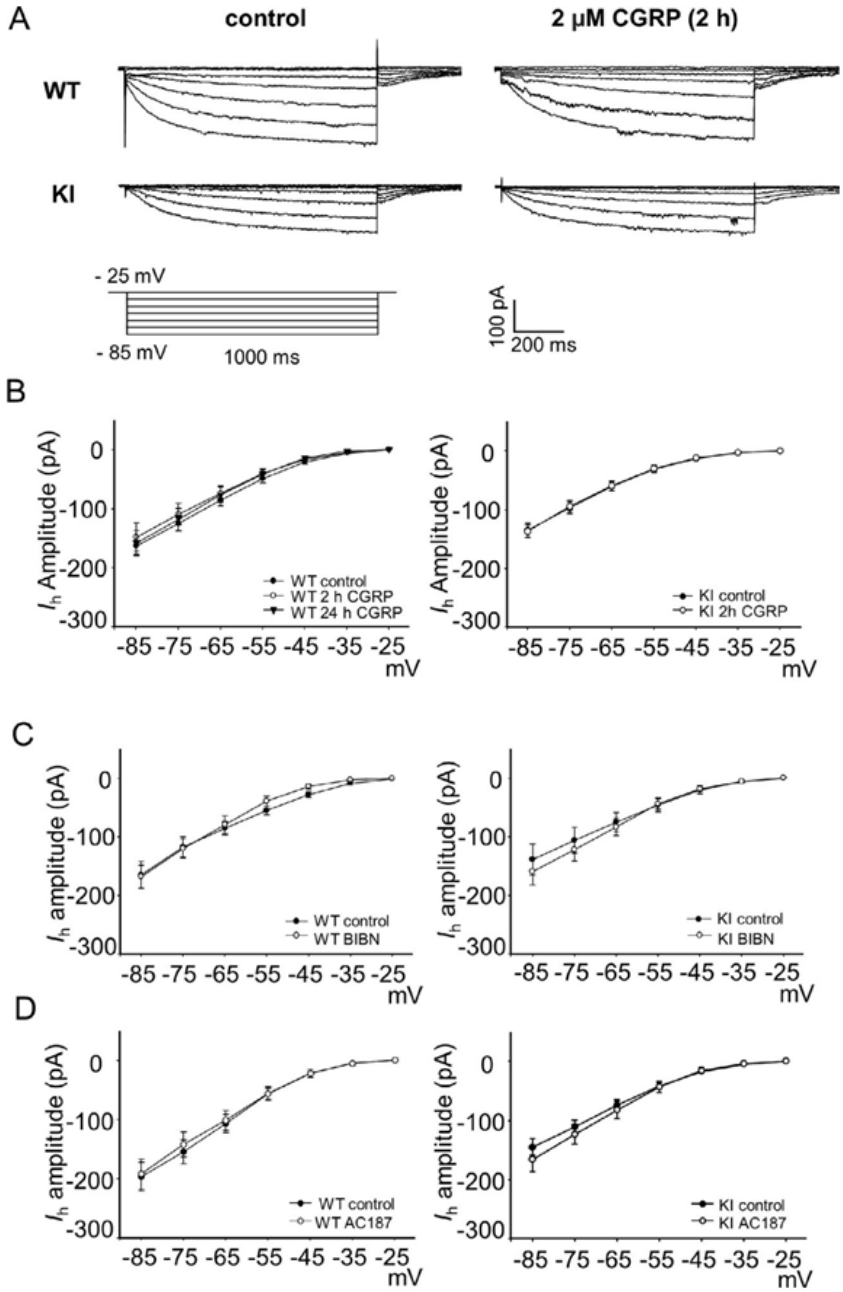

Fig. 4. Lack of effect by CGRP application on Ih current in TG neurons. (A) representative traces of Ih current recorded from KI and WT trigeminal (TG) neurons in control condition (left) and after a 2-h application of CGRP (2 μM, right). (B) *I-V* curves of average I_h current amplitude recorded from WT (left panel) and KI neurons (right panel) in control and after 2 or 24 h of CGRP application (KI control, n = 32; KI 2 h CGRP, n = 35; WT control, n = 37; WT 2 h CGRP, n = 26; WT 24 h CGRP, n = 22). (C) *I–V* curves of average *Ih* current amplitude recorded from WT (left panel) and KI neurons (right panel) in control and after a 24-h application of 50 nM BIBN 4096 (WT control, n = 12; WT BIBN, n = 11; KI control, n = 11; KI BIBN, n = 20). (D) *I–V* curves of average I_h current amplitude recorded from WT (left panel) and KI neurons (right panel) in control and after a 24-h application of 1 μM AC187 (KI control, n = 21; KI AC187, n = 22; WT control, n = 24; WT AC187, n = 21).

I_h current contribution to firing of WT and R192Q KI ganglion neurons

To explore how I_h activation could affect AP firing of KI and WT neurons, we studied, on the same cells, the evoked firing in control conditions first and then following application of ZD7288. TG neurons generate distinct firing patterns induced by activation of P2X3 or TRPV1 receptors (Hullugundi et al., 2014; Marchenkova et al., 2016a), which are both ionotropic receptors primarily mediating nociceptive transduction (Bradbury et al., 1998; Barclay et al., 2002; Meents et al., 2010; Nair et al., 2010) in physiological or pathological states (Nair et al., 2010; Yan and Dussor, 2014). Most neurons express functional P2X3 receptors, while TRPV1 channels are detected in approximately 50% TG neurons (Simonetti et al., 2006). Under basal conditions WT or KI neurons had 8.09 ± 0.6 or 9.19 ± 0.8 GΩ input resistance (n = 35 or 29, respectively), values substantially larger than those recorded under voltage-clamp configuration and attributable to the use of K-gluconate intracellular solution to reduce membrane leak components. We investigated the effect of I_h current inhibition on neuronal firing elicited by pulse application of the P2X3 agonist α,β-meATP or the TRPV1 agonist capsaicin to neurons held at –70 mV (Fig. 5). Fig. 5A shows representative traces of neuronal firing evoked by α,β-meATP (10 μM; 2 s) that elicited membrane depolarization associated with a cluster of APs on the rising phase of the response (Hullugundi et al., 2014). ZD7288 (50 μM; 5 min) reduced the number of spikes in both KI and WT neurons (Fig. 5A) without altering the amplitude of the P2X3-mediated depolarization (KI: 23.1 ± 1.9 mV in control *vs*. 22.9 ± 1.8 mV after ZD7288, n = 20; p = 0.83; WT: 33.3 ± 1.5 mV in control vs. 31.1 ± 1.5 mV after ZD7288, n = 28; p = 0.08). The difference in the amplitude of α,β-meATP-mediated depolarization between KI and WT neurons could be accounted for by the more negative firing threshold of KI cells that curtailed their purinergic response peak size. The firing pattern distribution was analyzed in KI and WT cultures (Fig. 5 B). As previously reported (Marchenkova et al., 2016a), KI cultures showed a much larger number of multiple-firing (MF) neurons and decreased number of non-spiking (NS) and single-spike (SS) neurons compared to WT. It is noteworthy that ZD7288 treatment converted the firing pattern of WT and KI neurons in a similar fashion with low presence of MF cells (Fig. 5 B).

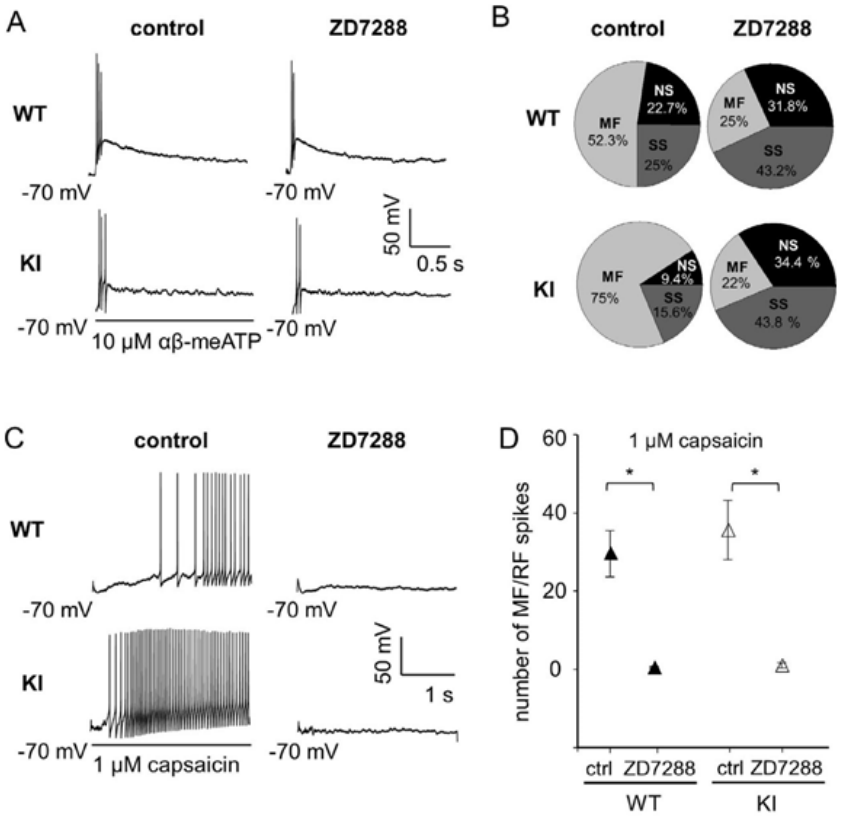

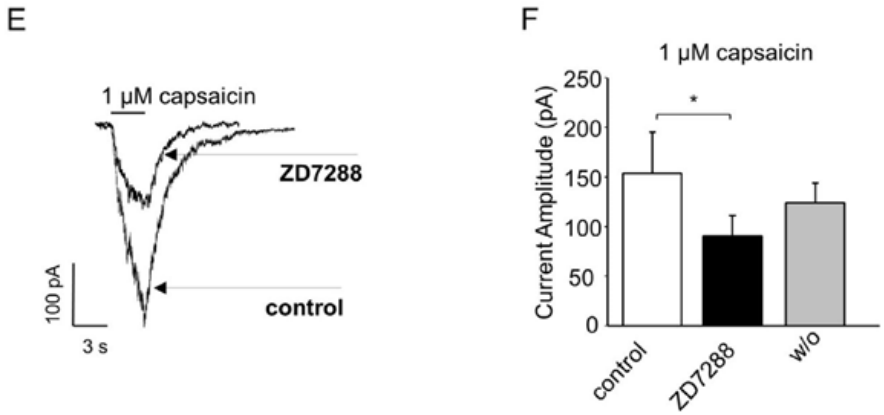

Fig. 5. *Ih* current blocker ZD7288 decreases the number of spikes evoked by α,β-meATP or capsaicin in R192Q KI and WT TG neurons. (A) representative traces of firing patterns recorded from KI and WT trigeminal ganglia (TG) neurons in response to 2-s pulses of 10 μM α,β-meATP in control condition (left) and after ZD7288 application (5 min, 50 μM; right) to the same cells. (B) pie charts for distribution of firing patterns among WT or KI TG neurons before (control) or after application of ZD7288. Note larger number of MF neurons in control KI (bottom left) compared to WT (upper left) cultures (p = 0.05, chi-square test). Right, pie charts show percent firing pattern distribution after ZD7288 application (WT: MF group, control vs ZD288 p = 0.009; KI: NS group, control vs ZD7288 p = 0.2, MF group, control vs ZD7288 p < 0.0001, SS group, control vs ZD7288 p = 0.01, chi-square test). Cell numbers for NS, MF and SS groups are, respectively: WT control, n=10, 23, 11; WT after ZD7288 application, n=14, 11, 19; KI control, n=3, 24, 5; KI after ZD7288 application, n = 11, 7, 14. Firing refers to average spike counts for α,β-meATPevoked effects. (C) Representative traces of firing patterns evoked by 1-μM capsaicin pulses (3 s) in KI and WT neurons in control (left) and after ZD7288 application (5 min, 50 μM; right) to the same cells. (D) Average spike counts for MF/RF neurons (which are the largest capsaicin-sensitive group) induced by capsaicin on KI (open triangles) and WT (filled triangles) neurons in control and after ZD7288; KI, n = 9, p = 0.0004; WT, n = 9, p = 0.0004, Mann–Whitney rank sum test. (E) Example of superimposed currents evoked by 1-mM capsaicin pulses on WT neurons in control and after ZD7288 application (5 min, 50 μM) to the same cell. (F) Histogram shows average peak amplitude values of TRPV1-mediated responses in control and after ZD7288 application (5 min, 50 μM) to the same cells (n = 10), and a 5-min washout (n = 5); *p=0.03, paired t-test.

We next examined APs induced by capsaicin (1 μM; 3 s) that produced a slow, shallow depolarization with superimposed sustained discharge of APs, a response almost abolished by ZD7288 in KI and WT neurons (Fig. 5 C, D). This observation suggests that ZD7288 might block TRPV1 channels, so we explored TRPV1 currents in control solution and after applying ZD7288 as shown in Fig. 5E, F. Under voltageclamp condition, the amplitude of the capsaicin-evoked current was nearly halved by this blocker indicating an additional target of its effect manifested on a subpopulation of TG neurons that is sensitive to capsaicin. Under current-clamp conditions, application of ZD7288 hyperpolarized the membrane potential of all tested cells (KI: –70.8 ±0.4 mV in control *vs*. –74 ±0.8 mV after ZD7288, n =21; p = 0.00004; WT: –69.6 ±0.5 mV in control *vs.* –76.1±1.1 mV after ZD7288, n = 20, p = 0.000004). This effect was controlled by repolarizing cells with DC current injection to a steady –70 mV value. To ascertain the contribution of I_h current to firing threshold from –70 mV, we applied ZD7288 (Fig. 6). Fig. 6A shows, on a fast time base, the first AP elicited in response to an α,β-meATP pulse, highlighting how the WT threshold level in control (–38 mV) was shifted to –34 mV upon ZD7288 application. It is also noteworthy that the spike trajectory became slower as it changed from 2.43 mV/ms to 0.91 mV/ms in the presence of ZD7288: on average, the value of the spike trajectory of WT neurons was shifted from 2.51±0.3 mV/ms in control to 1.87±0.2 mV/ms after ZD7288 (n = 29; p = 0.05), thus, delaying spike initiation. Previous studies (Hullugundi et al., 2014; Marchenkova et al., 2016a) have shown that R192Q KI neurons display enhanced basal excitability associated with a lower threshold for P2X3-mediated firing. We validated that α,β-meATP-evoked spikes of KI neurons possessed a more negative threshold compared to WT neurons (Fig. 6A, B). Likewise, ZD7288 application raised the spike threshold from –40 to –35 mV with a corresponding shortening of the spike trajectory speed (from 1.44 mV/ms to 0.14 mV/ms in the example of Fig. 6A). On average, the spike trajectory value of KI cells (2.47 ±0.2 mV/ms) was similar to that of WT because the trajectory rate relies on measuring the membrane depolarization to threshold divided by the time to threshold: this value in KI cells was also decreased by ZD7288 (to 1.74±0.2 ms; n = 22; p = 0.007). It seemed, therefore, more useful to compare the latency to spike initiation between WT and KI cells: KI=12.5±1.2 ms and WT=16.6±1.9 ms, both values were significantly decreased after ZD7288 (21.5±3.8 ms and 22.3 ±2.2 ms, respectively; p=0.009 and p=0.04; n=22 and 30 cells). On a small number of neurons (KI: n = 4 of 13 capsaicin-responsive neurons; WT: n = 5 of 12), it was possible to observe firing even after ZD7288, as exemplified in Fig. 6D and summarized in Fig. 6C. In these cells the Ih current inhibitor did not alter spike threshold of TRPV1-mediated neuronal firing (Fig. 6 C).

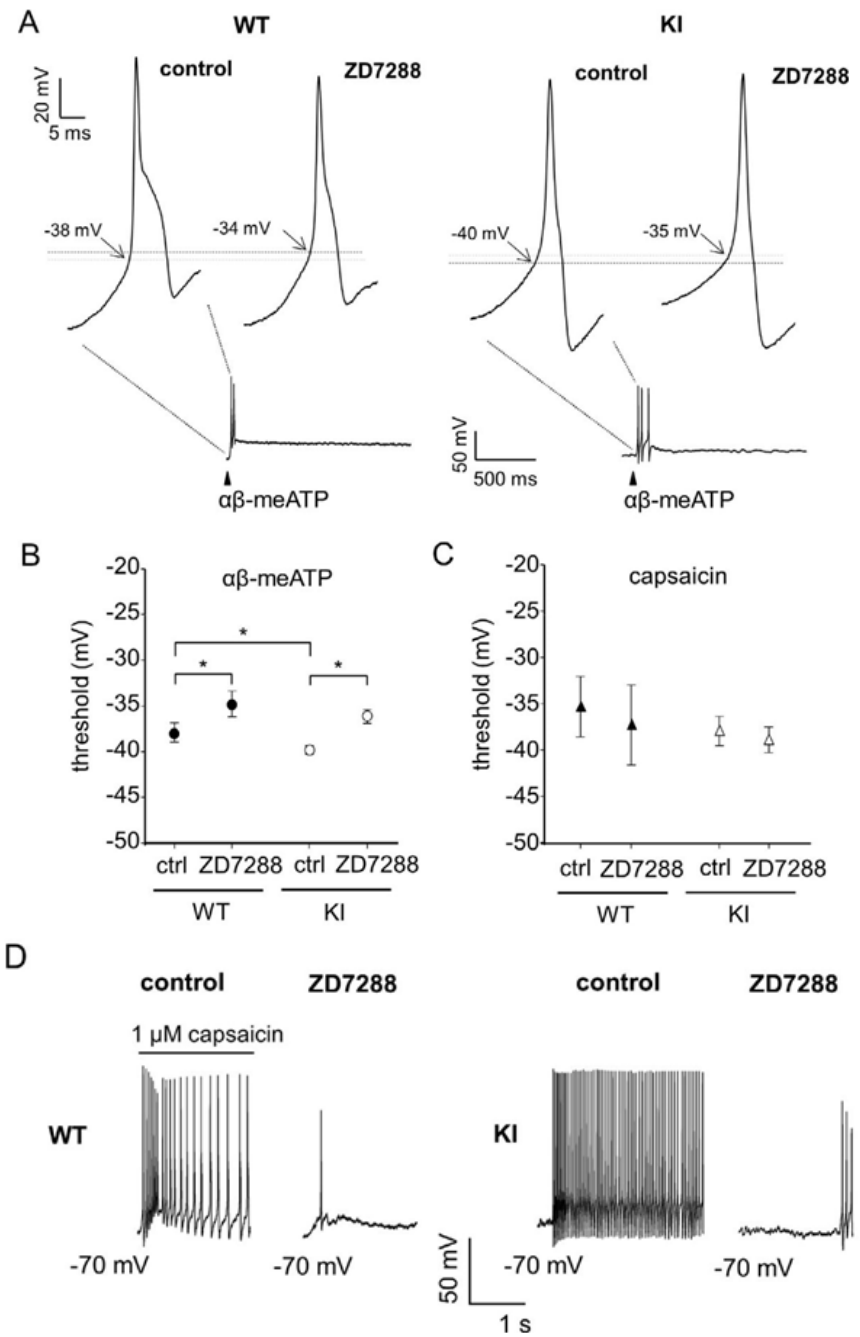

Fig. 6. Effect of I_h current blocker ZD7288 application on AP firing threshold evoked by α,β-meATP or capsaicin in R192Q KI and WT TG neurons. (A) Representative traces of first AP induced by α,β-meATP (2 s,10 μM) on KI and WT neurons in control condition and after ZD7288 (5 min, 50 μM); arrows indicate firing threshold. Same cells before and after ZD7288 application. Note the ZD7288-mediated shift of the AP threshold toward more positive values. (B–C) Diagrams show average threshold values of firing evoked by α,β-meATP (B: KI n = 25, *p = 0.00002 *vs* drug treated; WT n = 34, *p = 0.006 *vs* drug treated, paired t-test; control WT vs control KI *p = 0.01) or capsaicin pulses (C: KI, n = 4;WT, n = 5) for KI and WT neurons, in control and after ZD7288 application to the same cells. (D) Representative traces of TRPV1-mediated firing induced by capsaicin pulses (1 μM, 3 s) in control and after ZD7288 treatment (5 min, 50 μM) from WT (left) and KI (right) neurons. The traces are an example of those few neurons in which it was possible to observe capsaicin-induced firing even after ZD7288 application.

HCN subunit expression in mouse TG

Because of the reported heterogeneity of HCN channels with distinct expression and functional properties (reviewed in Biel et al., 2009), we used HCN isoformspecific polyclonal antibodies to study the distribution of the four HCN channel isoforms in the mouse TG using Western blot analysis (Fig. 7 A). Bands immunoreactive for each of the HCN subtypes were detected in mouse TG around the corresponding molecular mass seen in mouse olfactory bulb (Fig. 7 A). HCN2 antibody showed several bands

in olfactory bulb, but only one band in TG tissue, at a molecular weight (∼130 kDa) slightly lower than the higher bands observed in olfactory bulb (Fig. 7 A).

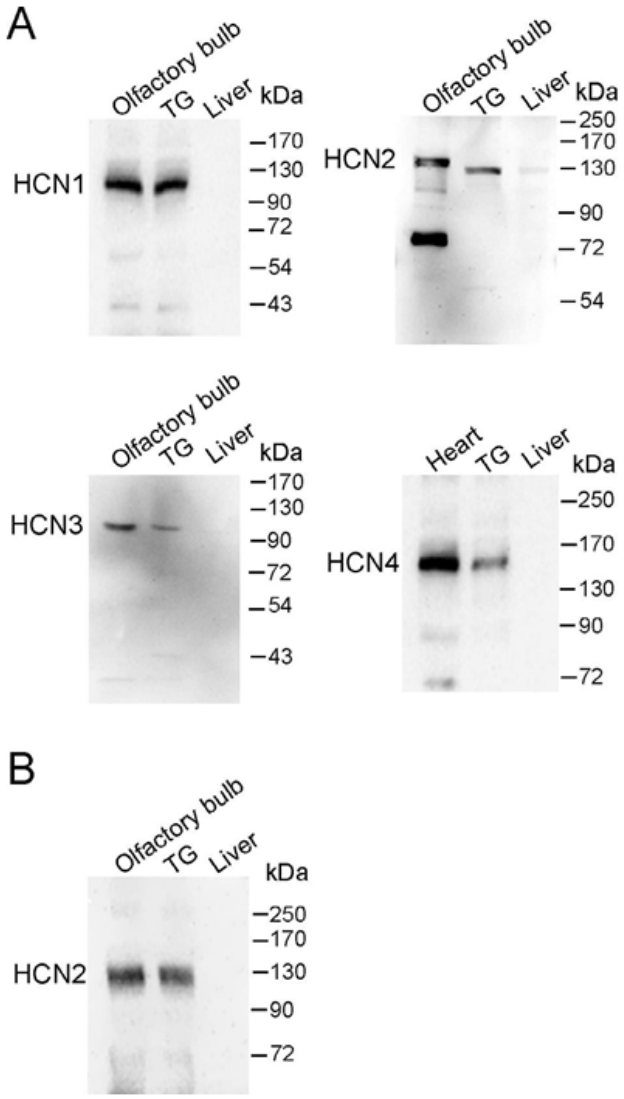

Fig. 7. Western blot analysis of mouse HCN subtypes in mouse TG. (A) representative example of Western blot showing HCN1, -2, -3 and -4 isoforms in whole-TG lysate from adult mice (lane 2 in each panel). Tissue lysate from olfactory bulb (lane 1) was used as positive control and liver (line 3) was used as negative control for evaluating antibody specificity. For HCN4, control-positive sample was heart tissue. (B) Western blots show lysates from olfactory bulb or TG cultures (TG) probed with anti-HCN2 antibodies. Lysates were incubated with Peptide-N-Glycosidase F (PNGase F) according to the manufacturer's instructions (New England Biolabs; 1000 u/reaction) to remove glycosylated products.

After removing the N-glycosylation moiety of the protein with PNGase F treatment (Tarentino et al., 1985), only one band was visible in the olfactory bulb sample at the same molecular weight as in TG lysate (Fig. 7 B). This suggests that the higher molecular weight HCN2 bands observed in olfactory bulb are likely due to the Nglycosylated forms.

Immunohistochemical preparations obtained from WT TG in situ showed that all the HCN subunits were present in TG neurons (labeled by the neuronal specific marker β-tubulin, Fig. 8A): immunostaining was concentrated to a ring-like structure beneath the cell membrane with weaker staining in cytoplasm, consistent with previous studies (Wells et al., 2007; Cho et al., 2009). Few neurons showed exclusively cytoplasmic staining for HCN1—3, whereas there was no cytoplasmic-only staining for HCN4. HCN1 and HCN2 were the isoforms most frequently expressed (58 ±2.3% and 50±4.6%, respectively), while HCN3 and HCN4 were expressed in a relatively small proportion of neurons (25 ±3.7% and 17±1.9%, respectively, Fig. 8 A). We took measurements of the neuronal diameter to relate HCN isoform expression to the functional class of TG neuron. As shown in Fig. 8B, HCN1 channel immunoreactivity was located predominantly to medium- and large-size TG neurons. HCN2 and HCN3

labeling was observed in neurons of all sizes, while HCN4 had a more constrained size distribution profile as it was predominantly observed in small- and medium-sized neurons (Fig. 8B). Preabsorption controls for HCN primary antibodies with their specific blocking peptide, and all other negative controls (omission of primary antibody) yielded no immunoreactive signal (Fig. 8C).

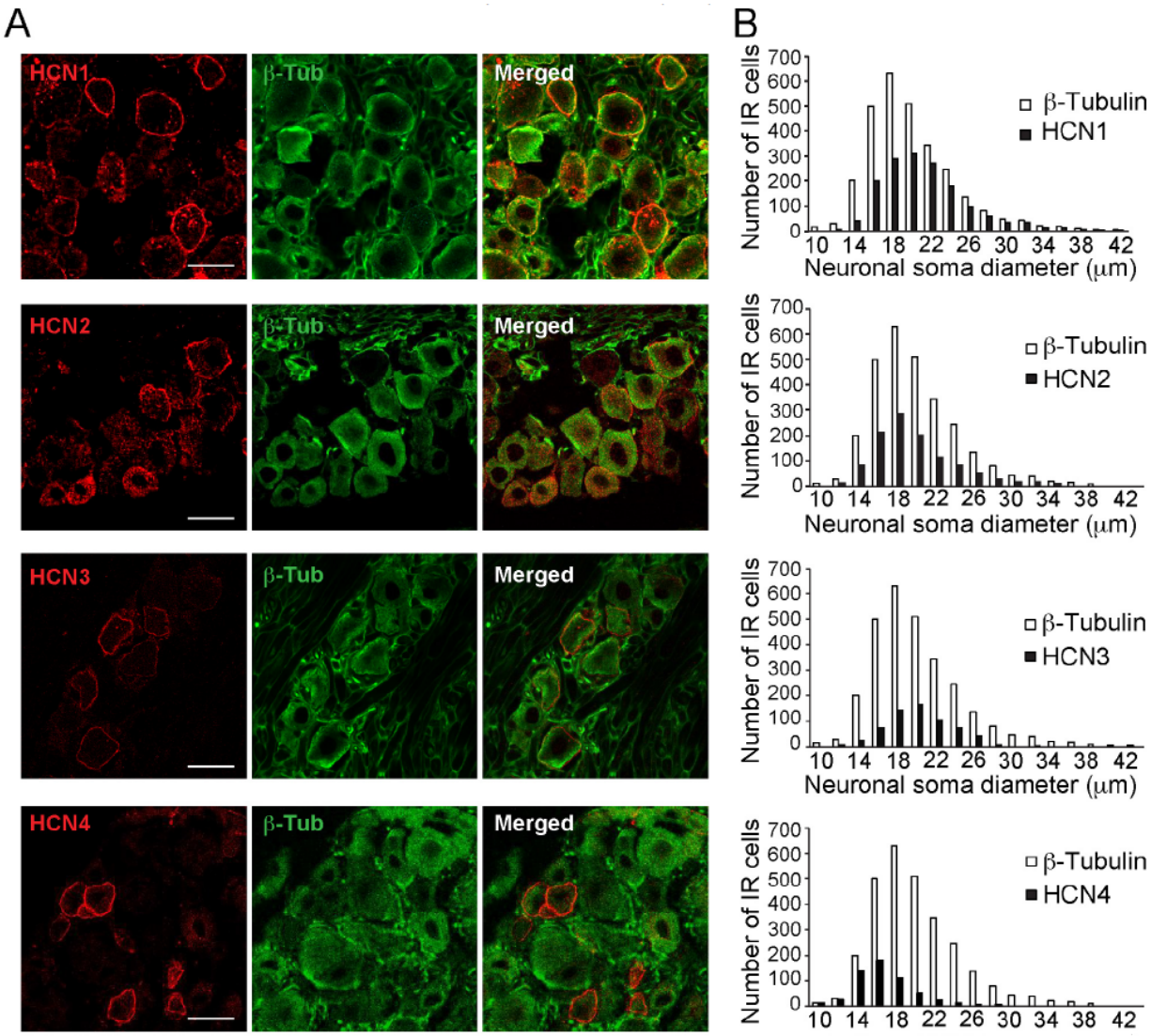

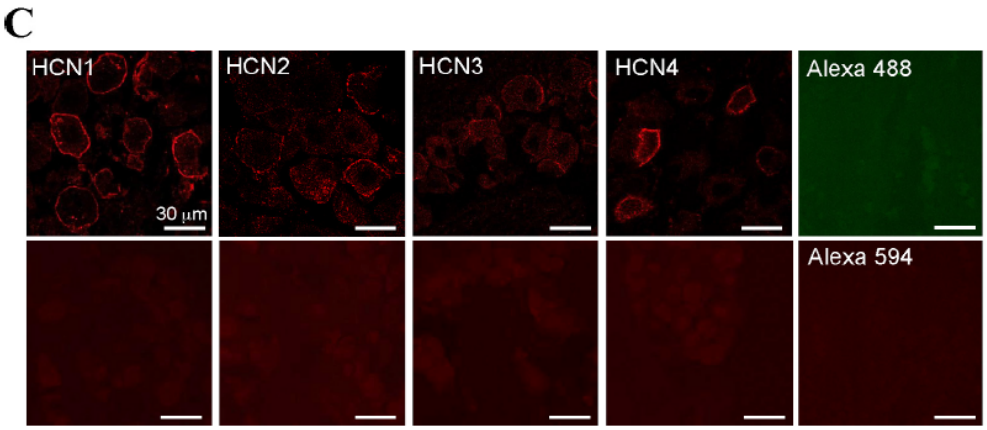

Fig. 8. Immunohistochemistry and size distributions of HCN channel subunits in mouse TG neurons *in situ*. (A) Representative micrographs showing examples of HCN1, -2, -3 or -4 (red) and β-tubulin (green) in longitudinal sections of adult TG. Cell nuclei are visualized with DAPI staining (blue). Note that the staining is predominantly on the cell surface membrane. Scale bar, 50 mm. (B) Histograms showing the size–frequency distribution of neurons immunoreactive for HCN1 or -2 or -3 or -4 (black), and β -tubulin (clear). (C) Pre-absorption controls showing that the distinctive HCN membrane staining (upper panels) was blocked when antibodies were pre-absorbed with excess of specific blocking peptide (lower panels). In negative controls (use of only the secondary antibodies Alexa 488 and Alexa 594), no immunoreactivity was observed. (For interpretation of the references to colour in this figure legend, the reader is referred to the web version of this article.)

HCN subunit expression in R192Q KI TG cultures

In vitro culturing conditions may have influenced I_h current characteristics compared to those that are present in the *in vivo* situation (Scroggs et al., 1994; Chaplan et al., 2003; Acosta et al., 2012). Therefore, we also investigated HCN isoform distribution in TG cultures (Fig. 9 A). Cell counting indicated that the proportion of WT TG neurons was 57 ± 3.6% immunopositive for HCN1, 50 ± 4.2% for HCN2, 23 ± 2.5% for HCN3 and 18 ± 4.3% for HCN4, thus confirming that the culturing conditions had not altered the relative proportion of HCN channel subunits in TG neurons. Regardless, HCN ring staining in TG neurons appeared much stronger *in vivo* than in culture, as previously reported (Acosta et al., 2012). A similar distribution of HCN channel subtype immunoreactive neurons was observed for TG cultures from KI mice, as shown in Fig. 9A and quantified in Fig. 9B. Western blot analysis did not show substantial differences in HCN sub-unit total levels found in KI or WT TG cultures (Fig. 9C).

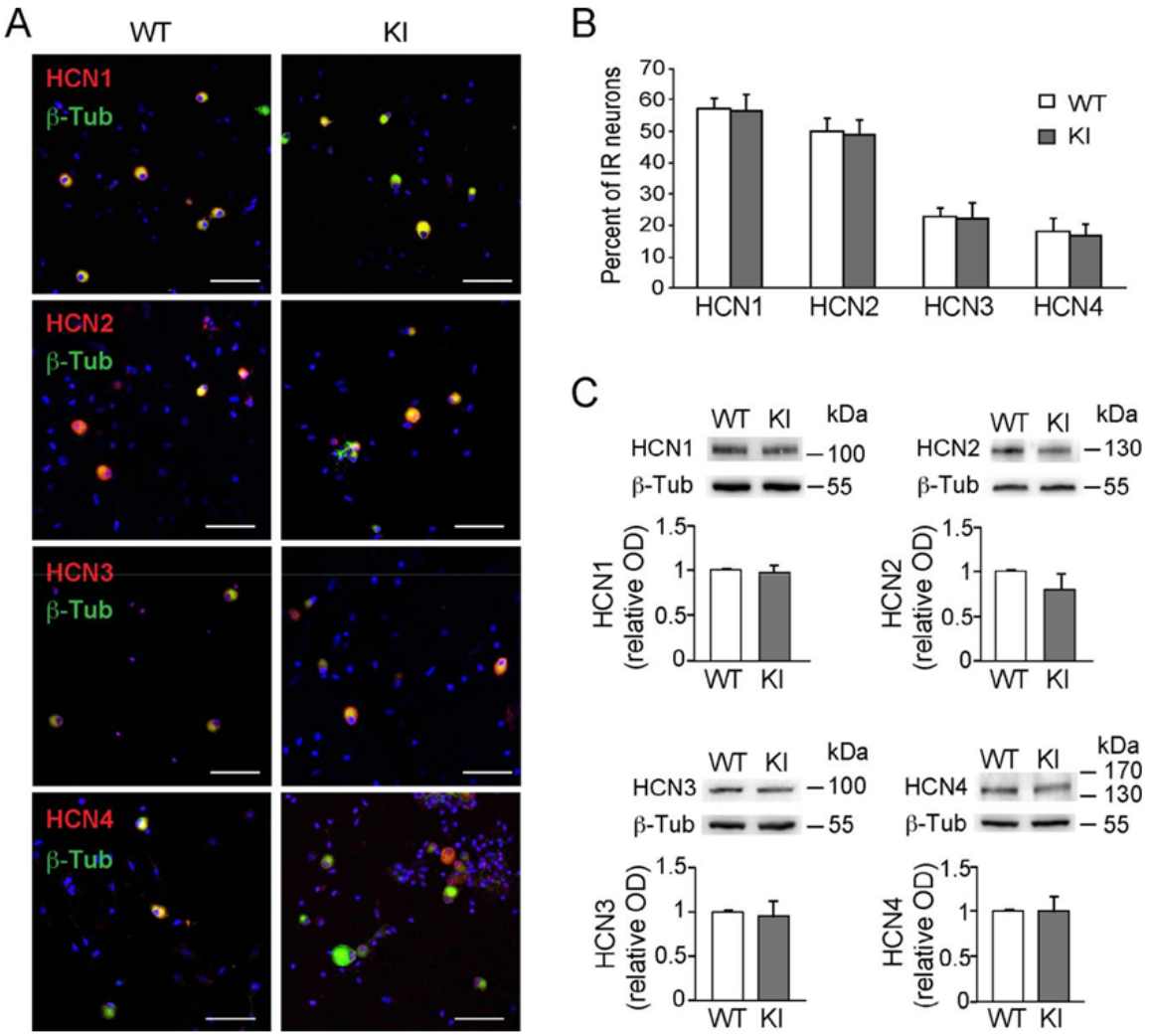

Fig. 9. Comparison of HCN channel subunit expression in TG cultures from R192Q KI and WT mice. (A) Representative immunocytochemical examples of endogenous HCN1, -2, -3 or -4 (red) and β-tubulin (green) in WT (left panels) and KI (right panels) TG cultures. Nuclei are visualized with DAPI (blue). Scale bar, 50 μm. (B) The histograms quantify percentage of HCN-positive cells in WT and KI (n = 500 neurons obtained from three independent experiments; $p < 0.05$). (C) Lysates of trigeminal ganglia from WT or KI mice were probed with antibodies to HCN1 or HCN2 or HCN3 or HCN4. In all Western blots, β-tubulin antibody was used as a loading control. Plots show the quantitative analysis of the band density (normalized to the tubulin band density). (For interpretation of the references to colour in this figure legend, the reader is referred to the web version of this article.)

Significant differences between cultured KI and WT TG neurons, however, emerged when investigating the cellular distribution of HCN subunits. Most strikingly, membrane biotinylation experiments showed a strong decrease (by nearly half as shown in Fig. 10A, top right) of membrane expression of HCN2 subunits in KI neurons. There was no apparent change in membrane expression of the HCN1, 3 and 4 subunits in the same samples (Fig. 10A).
To further explore the re-distribution of HCN2 subunits, confocal line-profile analysis of trigeminal neurons immunostained for HCN2 and β–tubulin was performed, as shown in Fig. 10B with examples of one WT (top) and one KI (bottom) neuron and related cell scan profiles. In WT neurons (n = 31), the HCN2 signal was concentrated as a ring along the cell membrane (Fig. 10 B), which resembles the neuronal staining pattern observed in intact ganglia (as exemplified in Fig. 8 A); the β-tubulin signal was uniformly distributed. In KI neurons (n = 37), HCN2 staining was present across the cell and largely decreased at the peri-membrane region, in accordance with a fall of cell surface expression as demonstrated in Fig. 10A (right).

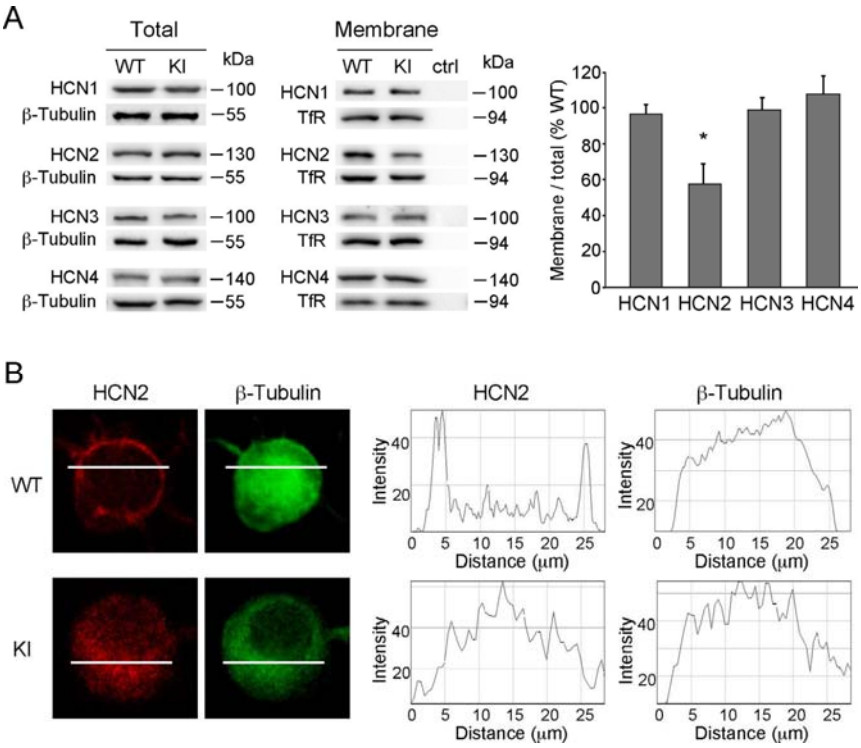

Fig. 10. Redistribution of HCN2 channels in R192Q KI TG neurons. (A) Examples of Western immunoblots (with the biotinylation procedure) showing the surface-expressed and total native HCN subunits in KI and WT TG cultures. The two left lanes represent total cellular HCN protein. The membrane lanes (right) represent biotinylated, plasma membrane-expressed channels (as supported by the presence of transferrin receptor TfR). The right lane is a negative control (ctrl) of streptavidin-immunoprecipitated samples without biotinylation. Lanes containing surface channels were loaded with 3 times the protein loaded for total protein analysis. Note the lower surface HCN2 channel expression in KI, with no significant change in HCN1, -3 and -4 surface expression. Histograms (right) quantify surface/total protein ratios for HCN subunits in KI TG cultures. Total HCN level was normalized with respect to β-tubulin as loading control. Values shown are mean s. d. (n = 4, $^*p < 0.05$). (B) Left, confocal microscopy images of single KI or WT cultured trigeminal neuron. Scale bar = 25 µm. Right, cell line-scan immunostaining profile for HCN2 or β-tubulin indicates sparse HCN2 immunostaining in KI. Similar results were obtained in at least three independent experiments (n = 37 KI cells, 31 WT cells).

DISCUSSION

The principal finding of the present study is the demonstration that R192Q KI TG neurons, despite their enhanced excitability, possess a smaller I_h current. This observation was consistent with re-distribution of the HCN2 subunits from the plasma membrane to the cytoplasmic compartment. This result might suggest a compensatory depression of I_h current to stabilize background neuronal activity so that triggering of trigeminal pain attacks could be produced only by stimuli like stress or strong light (Chanda et al., 2013).

I_h current in mouse TG neurons

The I_h current was readily observed in mouse TG neurons under voltage-clamp conditions using a standard protocol of voltage jumps that generate a slow inward current relaxation blocked by application of I_h inhibitor ZD7288. Identified I_h current characteristics were in line with those reported for other mammalian neurons (Maccaferri and McBain, 1996; Cho et al., 2011; Gao et al., 2012). At potentials near –40 mV, a value close to the current reversal (Maccaferri and McBain, 1996; Cho et al.,

2011; Gao et al., 2012), I_h-dependent relaxations disappeared, thus validating its role primarily in the sub-threshold region. Using TEA and lino-pirdine as pharmacological inhibitors of other voltage-activated K^+ conductances (Aiken et al., 1995; Passmore et al., 2003; Battefeld et al., 2012), it was apparent that the current relaxations recorded under the present experimental conditions were not largely contaminated by other K^+ currents, even if K^+ currents can be detected with depolarizing commands from resting potential (Spigelman and Puil, 1989).

With the present electrophysiological protocols, fast return of holding potential to -25 mV from more hyperpolarized values was only rarely accompanied by the emergence of an inward current (or a fast spike-like deflection) suggestive of transient activation of voltage-dependent Na^+ currents. This observation is consistent with several studies of sensory ganglion neurons in which the threshold for voltage-gated Na^+ currents is usually positive to –30 mV (Schlichter et al., 1991; Yoshimura and De Groat, 1996; Kim and Chung, 1999; Connor et al., 2005). Thus, although the present protocol of hyperpolarizing steps might have decreased inactivation of Na^+ currents at –25 mV holding potential, this approach per se was not suffcient to consistently generate Na^+ currents as off responses. Furthermore, low-threshold Na^+ currents reported for trigeminal sensory neurons are very prone to inactivation from which they recover very slowly since only 8 ± 3% current recovery is detected over a 5-min period of holding the membrane potential at –80 mV (Scroggs, 2012). Likewise, recovery from inactivation of high-threshold Na currents is also slow at standard membrane potential (–60 mV; Gotoh et al., 2002).

It was, however, unanticipated that KI TG neurons exhibited a significantly smaller I_h current at all tested potentials, even though the main properties of this current were similar to those found in WT neurons. Since the current difference between WT and KI neurons was present even at very negative membrane potential values (expected to express full I_h activation), this discrepancy did not simply reflect a shift in the activation curve of the channel in the two genotypes. This result led us to examine whether the higher constitutive release of neuropeptide CGRP, a typical migraine mediator (Olesen et al., 2004; Messlinger et al., 2011), previously detected in higher amount in KI ganglia (Ceruti et al., 2011; Fioretti et al., 2011), might have been the origin for the genotypic difference in activity of I_h current. Neither pre-treatment with CGRP nor application of its selective antagonist BIBN changed I_h currents in WT or KI neurons. Since CGRP may also act on a distinct subgroup of amylin-sensitive TG receptors, we also tested whether the selective amylin antagonist AC187 (Jhamandas et al., 2003) could alter I_h current, but observed no change. We, therefore, conclude that CGRP did not modulate the I_h current in WT or KI TG cells.

I_h current role in spike generation

Under current-clamp conditions, we studied changes in APs elicited by pulse application of the metabolically stable P2X3 agonist α,β-meATP (Jarvis and Khakh, 2009) or the TRPV1 agonist capsaicin (Caterina et al., 1997). The I_h current inhibitor ZD7288 significantly decreased the number of spikes evoked by either stimulus, an effect particularly strong for capsaicin responses as ZD7288 depressed TRPV1 currents while sparing P2X3 receptor-dependent depolarizations. Inspection of the spike trajectory (dV/dt) taken as a simple index of sub-threshold excitability in control solution showed that, on average, not only the spike threshold of KI neurons was more negative, but it also required significantly less time to reach firing. It should be noted that the spike threshold was usually more negative than the threshold for the fast Na^+ current activation: this difference is attributable to the use of the K-gluconate intracellular solution for the current-clamp experiments, a procedure that substantially increased the cell input resistance.

The smaller magnitude of I_h current detected in KI neurons was not inconsistent with the observed enhanced excitability phenotype, an effect similar to that observed when HCN2 is lacking even though the underlying mechanism remains poorly understood (Berger et al., 2003; Ludwig et al., 2003; Ying et al., 2012). After application of ZD7288, the spike threshold was raised in KI and WT neurons to a comparable level, suggesting that, despite different current amplitudes, I_h currents provided a contribution to either genotype.

The quantitatively distinct role of I_h in controlling spike generation in WT vs KI cells remains complex and not fully resolved. In fact, differences in excitability are apparent when firing is chemically evoked by P2X3 agonists or capsaicin, and absent when the stimuli are step depolarizing commands (Hullugundi et al., 2014). This issue raises the question of the differential time course of the applied stimulus (virtually instantaneous with current pulses or slower with chemicals) that likely impacts on the relative activation/deactivation kinetics of I_h that are quite different from those, for example, of P2X3 receptors (their desensitization time constant is approximately 100 ms; Sokolova et al., 2006). In addition, since the basal input resistance of WT and KI neurons is similar (Hullugundi et al., 2014) and unaffected by ZD7288, it is likely that the constitutive contribution by I_h to this parameter is small in keeping with the high input resistance of such cells.

Expression and distribution of HCN subunits

All four HCN subunits were expressed by TG ganglia *in situ* and in culture. In accordance with earlier studies (Chaplan et al., 2003; Kouranova et al., 2008; Hatch et al., 2013), HCN1 and -2 were most abundantly expressed and detected in the vast majority of TG neurons, a phenomenon preserved when TG neurons were cultured. It was interesting to note that HCN subunits were also strongly expressed at the level of neuronal processes, a result suggesting their potential to regulate the signal flow from afferent fibers to the cell body. Because of antibody cross-reactivity, it was not possible to dissect whether these subunits were present as homomeric and/ or heteromeric channels, which is relevant as they are known to require four channel proteins for functional activity ((Biel et al., 2009; He et al., 2014). However, due to the considerable overlap of distribution between HCN

isoforms, it is conceivable that I_h could be carried by heteromeric channels. Remarkably, in KI neurons more HCN2 was detectable in the cytoplasm (rather than at perimembrane level as seen for WT neurons). Since the overall expression of HCN channels was unchanged, the lower membrane expression of HCN2 in KI neurons might arise from reduced traffcking of this protein to the plasma membrane.

An interpretation for the differential expression and function of I_h by KI neurons

Previous studies of trigeminal sensory neurons have indicated that increased I_h leads to increased membrane excitability (Schlichter et al., 1991). Interestingly, I_h is selectively suppressed in herpes simplex-infected dorsal root ganglion neurons (Mayer, 1986), a phenomenon associated with a decrease in membrane excitability. These data accord with the notion that I_h promotes the excitability of trigeminal sensory neurons and is the pharmacological target of neurotransmitters such as serotonin (Chang et al., 2017). A former report has also indicated that genetic ablation of GABAergic tonic inhibition is associated with a strong, compensatory downregulation of I_h in hippocampal neurons (Bonin et al., 2013). It is, therefore, feasible to hypothesize a similar compensatory reduction in I_h expression and function by KI neurons because of the tonic increase in CGRP release and related hyperexcitability in this transgenic mouse model (Ceruti et al., 2011; Hullugundi et al., 2013) even if a direct link between these two phenomena was not found in the current study.

Our present findings accord with the notion that lower membrane expression of the HCN2 subunit in rat DRG neurons may correspond to impaired channel function (Acosta et al., 2012). The finding of low I_h expression by KI cells is not incompatible with the gain-of-function of $Ca_V2.1$ channels of such neurons (van den Maagdenberg et al., 2004; Nair et al., 2010) because the larger influx of Ca^{2+} can activate intracellular protein kinase C (Steinberg, 2008; Zeng et al., 2012) which in turn down-regulates HCN2 channel expression (reviewed by He et al., 2014). Recent studies of hippocampal neurons in culture have indicated that PKC inhibits the transport of HCN channel surface expression without altering their synthesis (Williams et al., 2015). The precise mechanisms controlling HCN subunit transport and turnover will require further investigation. There is growing evidence that HCN channels can form macromolecular protein complexes that, in addition to the principal pore-forming subunits, contain auxiliary proteins required for the fine-tuning of electrophysiological properties, the functional coupling to signaling pathways, and traffcking to specific cellular compartments (He et al., 2014). Recently, several proteins interacting with HCN channels have been identified (reviewed in (Biel et al., 2009; He et al., 2014) with multifarious functions in the up or down-regulation of all HCN isoforms or subunit-specific interactions. In particular, one can propose that certain scaffold proteins interact with the C-terminus of HCN channels to regulate channel targeting to distinct subcellular compartments (e.g. synapses or dendrites). In fact, a brain-specific protein termed TRIP8b is known to bind to the C- terminus of HCN channels (Santoro et al., 2004) with subsequent upregulation of these channels at the plasma membrane level. In addition, HCN2 (but not other HCN channels) interacts with the neuronal scaffold proteins tamalin and Mint2 (Kimura et al., 2004) that, at least in recombinant systems, upregulate HCN2 at the cell surface level (Kimura et al., 2004).

Furthermore, at membrane level direct interactions of voltage-gated channels with HCN channels can shape the function of I_h. For example, in forebrain neurons a subpopulation of leak K^+ channels termed TASK3 is thought to be negatively coupled to HCN2 channels (Meuth et al., 2006): thus, a pharmacological block of I_h current with ZD7288 may unmask the hyperpolarizing role of TASK3 channels and induce membrane potential hyperpolarization (Meuth et al., 2006). The present observations on TG neurons hyperpolarized by ZD7288 accord with the report of TRESK expression in sensory ganglia (Medhurst et al., 2001). Thus, it is likely that HCN2 function depends on the fine balance among various neuronal proteins tightly regulating, in a positive or negative fashion, the channel expression at membrane level.

CONCLUSIONS

Our data can help to propose I_h downregulation as one constitutive mechanism responsible for stabilizing neuronal sensory activity to prevent frequent attacks of trigeminal pain triggered by external stimuli in this mouse model of migraine. This process might be a compensatory action to contrast lack of basal inhibition by the neuropeptide brain natriuretic peptide (BNP; Marchenkova et al., 2016b), an important contributing factor to TG neuronal excitability under resting conditions.

Acknowledgments — This work was supported by the EU FP7 grant Euroheadpain (#602633).

All authors approved the final manuscript. Conception and design of the work FE, SV, AN; acquisition and analysis of data, FE, SV; interpretation of data, FE, SV, AvdM, AN; wrote/revised the manuscript, FE, SV, AvdM, AN.

The authors declare no competing interests.

REFERENCES

Acosta C, McMullan S, Djouhri L, Gao L, Watkins R, Berry C, Dempsey K, Lawson SN (2012) HCN1 and HCN2 in Rat DRG neurons: levels in nociceptors and non-nociceptors, NT3-dependence and influence of CFA-induced skin inflammation on HCN2 and NT3 expression. PLoS One 7:e50442.

Aiken SP, Lampe BJ, Murphy PA, Brown BS (1995) Reduction of spike frequency adaptation and blockade of M-current in rat CA1 pyramidal neurones by linopirdine (DuP 996), a neurotransmitter release enhancer. Br J Pharmacol 115:1163–1168.

Arroyo A, Kim B, Rasmusson RL, Bett G, Yeh J (2006) Hyperpolarization-activated cation channels are expressed in rat hypothalamic gonadotropin-releasing hormone (GnRH) neurons and immortalized GnRH neurons. J Soc Gynecol Investig 13:442–450.

Barclay J, Patel S, Dorn G, Wotherspoon G, Moffatt S, Eunson L, Abdel'al S, Natt F, Hall J, Winter J, Bevan S, Wishart W, Fox A, Ganju P (2002) Functional downregulation of P2X3 receptor subunit in rat sensory neurons reveals a significant role in chronic neuropathic and inflammatory pain. J Neurosci 22:8139–8147.

Battefeld A, Rocha N, Stadler K, Bra¨uer AU, Strauss U (2012) Distinct perinatal features of the hyperpolarization-activated non-selective cation current I_h in the rat cortical plate. Neural Dev 7:21.

Bean BP (2007) The action potential in mammalian central neurons. Nat Rev Neurosci 8:451–465.

Berger T, Senn W, Luscher H-R (2003) Hyperpolarization-activated current I_h disconnects somatic and dendritic spike initiation zones in layer V pyramidal neurons. J Neurophysiol 90:2428–2437.

Biel M, Wahl-Schott C, Michalakis S, Zong X (2009) Hyperpolarization-activated cation channels: from genes to function. Physiol Rev 89:847–885.

Bonin RP, Zurek AA, Yu J, Bayliss DA, Orser BA (2013) Hyperpolarization-activated current (I_h) is reduced in hippocampal neurons from Gabra5-/- mice. PLoS One 8:e58679.

BoSmith RE, Briggs I, Sturgess NC (1993) Inhibitory actions of ZENECA ZD7288 on whole-cell hyperpolarization activated inward current (I_f) in guinea-pig dissociated sinoatrial node cells. Br J Pharmacol 110:343–349.

Bradbury EJ, Burnstock G, McMahon SB (1998) The expression of P2X3 purinoreceptors in sensory neurons: effects of axotomy and glial-derived neurotrophic factor. Mol Cell Neurosci 12:256–268.

Caterina MJ, Schumacher MA, Tominaga M, Rosen TA, Levine JD, Julius D (1997) The capsaicin receptor: a heat-activated ion channel in the pain pathway. Nature 389:816–824.

Ceruti S, Villa G, Fumagalli M, Colombo L, Magni G, Zanardelli M, Fabbretti E, Verderio C, van den Maagdenberg AM, Nistri A, Abbracchio MP (2011) Calcitonin gene-related peptide-mediated enhancement of purinergic neuron/glia communication by the algogenic factor bradykinin in mouse trigeminal ganglia from wild-type and R192Q $Ca_v2.1$ knock-in mice: implications for basic mechanisms of migraine pain. J Neurosci 31:3638–3649.

Chanda ML, Tuttle AH, Baran I, Atlin C, Guindi D, Hathaway G, Israelian N, Levenstadt J, Low D, Macrae L, O'Shea L, Silver A, Zendegui E, Mariette Lenselink A, Spijker S, Ferrari MD, van den Maagdenberg AMJM, Mogil JS (2013) Behavioral evidence for photophobia and stress-related ipsilateral head pain in transgenic Cacna1a mutant mice. Pain 154:1254–1262.

Chang W, Kanda H, Ikeda R, Ling J, Gu JG (2017) Serotonergic transmission at Merkel discs: modulation by exogenously applied chemical messengers and involvement of I_h currents. J Neurochem. http://dx.doi.org/10.1111/jnc.14009.

Chaplan SR, Guo H-Q, Lee DH, Luo L, Liu C, Kuei C, Velumian AA, Butler MP, Brown SM, Dubin AE (2003) Neuronal hyperpolarization-activated pacemaker channels drive neuropathic pain. J Neurosci 23:1169–1178.

Cho H, Staikopoulos V, Ivanusic JJ, Jennings EA (2009) Hyperpolarization-activated cyclic-nucleotide gated 4 (HCN4) protein is expressed in a subset of rat dorsal root and trigeminal ganglion neurons. Cell Tissue Res 338:171–177.

Cho H-J, Furness JB, Jennings EA (2011) Postnatal maturation of the hyperpolarization-activated cation current, I_h, in trigeminal sensory neurons. J Neurophysiol 106:2045–2056.

Connor M, Naves LA, McCleskey EW (2005) Contrasting phenotypes of putative proprioceptive and nociceptive trigeminal neurons innervating jaw muscle in rat. Mol Pain 1:31.

Eikermann-Haerter K, Dileko¨z E, Kudo C, Savitz SI, Waeber C, Baum MJ, Ferrari MD, van den Maagdenberg AM, Moskowitz MA, Ayata C (2009) Genetic and hormonal factors modulate spreading depression and transient hemiparesis in mouse models of familial hemiplegic migraine type 1. J Clin Invest 119:99–109.

Emery EC, Young GT, Berrocoso EM, Chen L, McNaughton PA (2011) HCN2 ion channels play a central role in inflammatory and neuropathic pain. Science 333:1462–1466.

Emery EC, Young GT, McNaughton PA (2012) HCN2 ion channels: an emerging role as the pacemakers of pain. Trends Pharmacol Sci 33:456–463.

Fabbretti E, D'Arco M, Fabbro A, Simonetti M, Nistri A, Giniatullin R (2006) Delayed upregulation of ATP P2X3 receptors of trigeminal sensory neurons by calcitonin gene-related peptide. J Neurosci 26:6163–6171.

Fabbretti E, Sokolova E, Masten L, D'Arco M, Fabbro A, Nistri A, Giniatullin R (2004) Identification of negative residues in the P2X3 ATP receptor ectodomain as structural determinants for desensitization and the Ca^{2+}-sensing modulatory sites. J Biol Chem 279:53109–53115.

Ferrari MD, Klever RR, Terwindt GM, Ayata C, van den Maagdenberg AM (2015) Migraine pathophysiology: lessons from mouse models and human genetics. Lancet Neurol 14:65–80.

Fioretti B, Catacuzzeno L, Sforna L, Gerke-Duncan MB, van den Maagdenberg AM, Franciolini F, Connor M, Pietrobon D (2011) Trigeminal ganglion neuron subtype-specific alterations of $Ca_v2.1$ calcium current and excitability in a Cacna1a mouse model of migraine. J Physiol 589:5879–5895.

Funahashi M, Mitoh Y, Kohjitani A, Matsuo R (2003) Role of the hyperpolarization-activated cation current (I_h) in pacemaker activity in area postrema neurons of rat brain slices. J Physiol 552:135–148.

Gao LL, McMullan S, Djouhri L, Acosta C, Harper AA, Lawson SN (2012) Expression and properties of hyperpolarization-activated current in rat dorsal root ganglion neurons with known sensory function. J Physiol 590:4691–4705.

Gotoh M, Noro N, Sahara Y (2002) Kinetic properties of tetrodotoxin-sensitive and tetrodotoxin-resistant sodium channel currents in neonatal rat trigeminal ganglion neurons. J Med Dent Sci 49:43–55.

Halliwell JV, Adams PR (1982) Voltage-clamp analysis of muscarinic excitation in hippocampal neurons. Brain Res 250:71–92.

Han W, Bao W, Wang Z, Nattel S (2002) Comparison of ion-channel subunit expression in canine cardiac Purkinje fibers and ventricular muscle. Circ Res 91:790–797.

Harris NC, Constanti A (1995) Mechanism of block by ZD 7288 of the hyperpolarization-activated inward rectifying current in guinea pig substantia nigra neurons in vitro. J Neurophysiol 74:2366–2378.

Hatch RJ, Jennings EA, Ivanusic JJ (2013) Peripheral hyperpolarization-activated cyclic nucleotide-gated channels contribute to inflammation-induced hypersensitivity of the rat temporomandibular joint. Eur J Pain Lond Engl 17:972–982.

He C, Chen F, Li B, Hu Z (2014) Neurophysiology of HCN channels: from cellular functions to multiple regulations. Prog Neurobiol 112:1–23.

Headache Classification Committee of the International Headache Society (IHS) (2013) The International Classification of Headache Disorders, 3rd edition (beta version). Cephalalgia Int J Headache 33:629–808.

Hofmann F, Biel M, Kaupp UB (2005) International Union of Pharmacology. LI. Nomenclature and structure-function relationships of cyclic nucleotide-regulated channels. Pharmacol Rev 57:455–462.

Hullugundi SK, Ansuini A, Ferrari MD, van den Maagdenberg AM, Nistri A (2014) A hyperexcitability phenotype in mouse trigeminal sensory neurons expressing the R192Q Cacna1a missense mutation of familial hemiplegic migraine type-1. Neuroscience 266:244–254.

Hullugundi SK, Ferrari MD, van den Maagdenberg AM, Nistri A (2013) The mechanism of functional up-regulation of P2X3 receptors of trigeminal sensory neurons in a genetic mouse model of familial hemiplegic migraine type 1 (FHM-1). PLoS One 8:e60677.

Jarvis MF, Khakh BS (2009) ATP-gated P2X cation-channels. Neuropharmacology 56:208–215.

Jhamandas JH, Harris KH, Cho C, Fu W, MacTavish D (2003) Human amylin actions on rat cholinergic basal forebrain neurons: antagonism of beta-amyloid effects. J Neurophysiol 89:2923–2930. Julius D, Basbaum AI (2001) Molecular mechanisms of nociception. Nature 413:203–210.

Kim HC1, Chung MK (1999) Voltage-dependent sodium and calcium currents in acutely isolated adult rat trigeminal root ganglion neurons. J Neurophysiol 81:1123–1134.

Kimura K, Kitano J, Nakajima Y, Nakanishi S (2004) Hyperpolarization-activated, cyclic nucleotide-gated HCN2 cation channel forms a protein assembly with multiple neuronal scaffold proteins in distinct modes of protein-protein interactions. Genes Cells 9:631–640.

Kitagawa J, Takeda M, Suzuki I, Kadoi J, Tsuboi Y, Honda K, Matsumoto S, Nakagawa H, Tanabe A, Iwata K (2006) Mechanisms involved in modulation of trigeminal primary afferent activity in rats with peripheral mononeuropathy. Eur J Neurosci 24:1976–1986.

Kouranova EV, Strassle BW, Ring RH, Bowlby MR, Vasilyev DV (2008) Hyperpolarization-activated cyclic nucleotide-gated channel mRNA and protein expression in large versus small diameter dorsal root ganglion neurons: correlation with hyperpolarization-activated current gating. Neuroscience 153:1008–1019.

Lee DH, Chang L, Sorkin LS, Chaplan SR (2005) Hyperpolarization-activated, cation-nonselective, cyclic nucleotide-modulated channel blockade alleviates mechanical allodynia and suppresses ectopic discharge in spinal nerve ligated rats. J Pain 6:417–424.

Ludwig A, Budde T, Stieber J, Moosmang S, Wahl C, Holthoff K, Langebartels A, Wotjak C, Munsch T, Zong X, Feil S, Feil R, Lancel M, Chien KR, Konnerth A, Pape H-C, Biel M, Hofmann F (2003) Absence epilepsy and sinus dysrhythmia in mice lacking the pacemaker channel HCN2. EMBO J 22:216–224.

Ludwig A, Zong X, Jeglitsch M, Hofmann F, Biel M (1998) A family of hyperpolarization-activated mammalian cation channels. Nature 393:587–591.

Maccaferri G, Mangoni M, Lazzari A, DiFrancesco D (1993) Properties of the hyperpolarization-activated current in rat hippocampal CA1 pyramidal cells. J Neurophysiol 69:2129–2136.

Maccaferri G, McBain CJ (1996) The hyperpolarization-activated current (I_h) and its contribution to pacemaker activity in rat CA1 hippocampal stratum oriens-alveus interneurones. J Physiol 497 (Pt 1):119–130.

Marchenkova A, van den Maagdenberg AM, Nistri A (2016a) Loss of inhibition by brain natriuretic peptide over P2X3 receptors contributes to enhanced spike firing of trigeminal ganglion neurons in a mouse model of familial hemiplegic migraine type-1. Neuroscience 331:197–205.

Marchenkova A, Vilotti S, Ntamati N, van den Maagdenberg AM, Nistri A (2016b) Inefficient constitutive inhibition of P2X3 receptors by brain natriuretic peptide system contributes to sensitization of trigeminal sensory neurons in a genetic mouse model of familial hemiplegic migraine. Mol Pain 12:1–12.

Matsuyoshi H, Masuda N, Chancellor MB, Erickson VL, Hirao Y, de Groat WC, Wanaka A, Yoshimura N (2006) Expression of hyperpolarization-activated cyclic nucleotide-gated cation channels in rat dorsal root ganglion neurons innervating urinary bladder. Brain Res 1119:115–123.

Mayer ML (1986) Selective block of inward but not outward rectification in rat sensory neurones infected with herpes simplex virus. J Physiol 375:327–338.

Medhurst AD, Rennie G, Chapman CG, Meadows H, Duckworth MD, et al. (2001) Distribution analysis of human two pore domain potassium channels in tissues of the central nervous system and periphery. Brain Res Mol Brain Res 86:101–114.

Meents JE, Neeb L, Reuter U (2010) TRPV1 in migraine pathophysiology. Trends Mol Med 16:153–159.

Messlinger K, Fischer MJM, Lennerz JK (2011) Neuropeptide effects in the trigeminal system: pathophysiology and clinical relevance in migraine. Keio J Med 60:82–89.

Meuth SG, Kanyshkova T, Meuth P, Landgraf P, Munsch T, Ludwig A, Hofmann F, Pape H-C, Budde T (2006) Membrane resting potential of thalamocortical relay neurons is shaped by the interaction among TASK3 and HCN2 channels. J Neurophysiol 96:1517–1529.

Momin A, Cadiou H, Mason A, McNaughton PA (2008) Role of the hyperpolarization-activated current I_h in somatosensory neurons. J Physiol 586:5911–5929.

Moosmang S, Stieber J, Zong X, Biel M, Hofmann F, Ludwig A (2001) Cellular expression and functional characterization of four hyperpolarization-activated pacemaker channels in cardiac and neuronal tissues. Eur J Biochem 268:1646–1652.

Much B, Wahl-Schott C, Zong X, Schneider A, Baumann L, Moosmang S, Ludwig A, Biel M (2003) Role of subunit heteromerization and N-linked glycosylation in the formation of functional hyperpolarization-activated cyclic nucleotide-gated channels. J Biol Chem 278:43781–43786.

Nair A, Simonetti M, Birsa N, Ferrari van den MD, Maagdenberg AM, Giniatullin R, Nistri A, Fabbretti E (2010) Familial hemiplegic migraine Cav2.1 channel mutation R192Q enhances ATP-gated P2X3 receptor activity of mouse sensory ganglion neurons mediating trigeminal pain. Mol Pain 6:48.

North RA (2003) The P2X3 subunit: a molecular target in pain therapeutics. Curr Opin Investig Drugs Lond Engl 2000(4):833–840.

Notomi T, Shigemoto R (2004) Immunohistochemical localization of I_h channel subunits, HCN1-4, in the rat brain. J Comp Neurol 471:241–276.

Olesen J, Diener HC, Husstedt IW, Goadsby PJ, Hall D, Meier U, Pollentier S, Lesko LM, BIBN 4096 BS Clinical Proof of Concept Study Group (2004) Calcitonin gene-related peptide receptor antagonist BIBN 4096 BS for the acute treatment of migraine. N Engl J Med 350:1104–1110.

Ophoff RA, Terwindt GM, Vergouwe MN, van Eijk R, Oefner PJ, Hoffman SM, Lamerdin JE, Mohrenweiser HW, Bulman DE, Ferrari M, Haan J, Lindhout D, van Ommen GJ, Hofker MH, Ferrari MD, Frants RR (1996) Familial hemiplegic migraine and episodic ataxia type-2 are caused by mutations in the Ca^{2+} channel gene CACNL1A4. Cell 87:543–552.

Orio P, Madrid R, de la Pen˜a E, Parra A, Meseguer V, Bayliss DA, Belmonte C, Viana F (2009) Characteristics and physiological role of hyperpolarization activated currents in mouse cold thermoreceptors. J Physiol 587:1961–1976.

Passmore GM, Selyanko AA, Mistry M, Al-Qatari M, Marsh SJ, Matthews EA, Dickenson AH, Brown TA, Burbidge SA, Main M, Brown DA (2003) KCNQ/M currents in sensory neurons: significance for pain therapy. J Neurosci 23:7227–7236.

Platkiewicz J, Brette R (2010) A threshold equation for action potential initiation. PLoS Comput Biol 6:e1000850.

Puil E, Gimbarzevsky B, Miura RM (1987) Voltage dependence of membrane properties of trigeminal root ganglion neurons. J Neurophysiol 58:66–86.

Puil E, Gimbarzevsky B, Spigelman I (1988) Primary involvement of K+ conductance in membrane resonance of trigeminal root ganglion neurons. J Neurophysiol 59:77–89.

Robinson RB, Siegelbaum SA (2003) Hyperpolarization-activated cation currents: from molecules to physiological function. Annu Rev Physiol 65:453–480.

Santoro B, Liu DT, Yao H, Bartsch D, Kandel ER, Siegelbaum SA, Tibbs GR (1998) Identification of a gene encoding a hyperpolarization-activated pacemaker channel of brain. Cell 93:717–729.
Santoro B, Wainger BJ, Siegelbaum SA (2004) Regulation of HCN channel surface expression by a novel C-terminal protein-protein interaction. J Neurosci 24:10750–10762.

Schlichter R, Bader CR, Bernheim L (1991) Development of anomalous rectification (I_h) and of a tetrodotoxin-resistant sodium current in embryonic quail neurones. J Physiol 442:127–145.

Scroggs RS, Todorovic SM, Anderson EG, Fox AP (1994) Variation in I_H, I_{IR}, and I_{LEAK} between acutely isolated adult rat dorsal root ganglion neurons of different size. J Neurophysiol 71:271–279.

Scroggs RS (2012) The distribution of low-threshold TTX-resistant Na^+ currents in rat trigeminal ganglion cells. Neuroscience 222:205–214.

Sekerli M, Del Negro CA, Lee RH, Butera RJ (2004) Estimating action potential thresholds from neuronal time-series: new metrics and evaluation of methodologies. IEEE Trans Biomed Eng 51:1665–1672.

Simonetti M, Fabbro A, D'Arco M, Zweyer M, Nistri A, Giniatullin R, Fabbretti E (2006) Comparison of P2X and TRPV1 receptors in ganglia or primary culture of trigeminal neurons and their modulation by NGF or serotonin. Mol Pain 2:11.

Sokolova E, Skorinkin A, Moiseev I, Agrachev A, Nistri A, Giniatullin R (2006) Experimental and modeling studies of desensitization of P2X3 receptors. Mol Pharmacol 70:373–382.

Spigelman I, Puil E (1989) K+-channel blockade in trigeminal root ganglion neurons: effects on membrane outward currents. J Neurophysiol 62:802–809.

Steinberg SF (2008) Structural basis of protein kinase C isoform function. Physiol Rev 88:1341–1378.

Stieber J, Thomer A, Much B, Schneider A, Biel M, Hofmann F (2003) Molecular basis for the different activation kinetics of the pacemaker channels HCN2 and HCN4. J Biol Chem 278:33672–33680.

Tarentino AL, Go´mez CM, Plummer TH (1985) Deglycosylation of asparagine-linked glycans by peptide:N-glycosidase F. Biochemistry (Mosc) 24:4665–4671.

Tolner EA, Houben T, Terwindt GM, de Vries B, Ferrari MD, van den Maagdenberg AM (2015) From migraine genes to mechanisms. Pain 156(Suppl 1):S64–S74.

Tottene A, Conti R, Fabbro A, Vecchia D, Shapovalova M, Santello M, van den Maagdenberg AM, Ferrari MD, Pietrobon D (2009) Enhanced excitatory transmission at cortical synapses as the basis for facilitated spreading depression in $Ca_v2.1$ knockin migraine mice. Neuron 61:762–773.

Tsuboi Y, Takeda M, Tanimoto T, Ikeda M, Matsumoto S, Kitagawa J, Teramoto K, Simizu K, Yamazaki Y, Shima A, Ren K, Iwata K (2004) Alteration of the second branch of the trigeminal nerve activity following inferior alveolar nerve transection in rats. Pain 111:323–334.

Tu H, Deng L, Sun Q, Yao L, Han J-S, Wan Y (2004) Hyperpolarization-activated, cyclic nucleotide-gated cation channels: roles in the differential electrophysiological properties of rat primary afferent neurons. J Neurosci Res 76:713–722.

van den Maagdenberg AM, Pietrobon D, Pizzorusso T, Kaja S, Broos LA, Cesetti T, van de Ven RC, Tottene A, van der Kaa J, Plomp JJ, Frants RR, Ferrari MD (2004) A Cacna1a knockin migraine mouse model with increased susceptibility to cortical spreading depression. Neuron 41:701–710.

Vilotti S, Marchenkova A, Ntamati N, Nistri A (2013) B-type natriuretic peptide-induced delayed modulation of TRPV1 and P2X3 receptors of mouse trigeminal sensory neurons. PLoS One 8: e81138.

Walker CS, Hay DL (2013) CGRP in the trigeminovascular system: a role for CGRP, adrenomedullin and amylin receptors? Br J Pharmacol 170:1293–1307.

Wells JE, Rowland KC, Proctor EK (2007) Hyperpolarization-activated channels in trigeminal ganglia innervating healthy and pulp-exposed teeth. Int Endod J 40:715–721.

Weng X, Smith T, Sathish J, Djouhri L (2012) Chronic inflammatory pain is associated with increased excitability and hyperpolarization-activated current (I_h) in C- but not Ad-nociceptors. Pain 153:900–914.

Williams AD, Jung S, Poolos NP (2015) Protein kinase C bidirectionally modulates Ih and hyperpolarization-activated cyclic nucleotide-gated (HCN) channel surface expression in hippocampal pyramidal neurons. J Physiol 593:2779–2792.

Wimalawansa SJ (1997) Amylin, calcitonin gene-related peptide, calcitonin, and adrenomedullin: a peptide superfamily. Crit Rev Neurobiol 11:167–239.

Yan J, Dussor G (2014) Ion channels and migraine. Headache 54:619–639.

Yao H, Donnelly DF, Ma C, LaMotte RH (2003) Upregulation of the hyperpolarization-activated cation current after chronic compression of the dorsal root ganglion. J Neurosci 23:2069–2074.

Ying S-W, Kanda VA, Hu Z, Purtell K, King EC, Abbott GW, Goldstein PA (2012) Targeted deletion of Kcne2 impairs HCN channel function in mouse thalamocortical circuits. PLoS One 7:e42756.

Yoshimura N, De Groat WC (1996) Characterization of voltage-sensitive Na^+ and K^+ currents recorded from acutely dissociated pelvic ganglion neurons of the adult rat. J Neurophysiol 76:2508–2521.

Zeng L, Webster SV, Newton PM (2012) The biology of protein kinase C. Adv Exp Med Biol 740:639–661.